Journal of Renewable Energy and Sustainable Development (RESD) Volume 10, Issue 2, December 2024 - ISSN 2356-8569
http://dx.doi.org/10.21622/RESD.2024.10.2.933

Received on, 20 July 2024 Accepted on, 03 October 2024 Published on, 03 November 2024

Machine Learning Models for Predicting Spatiotemporal Dynamics of Groundwater Recharge

Azeddine ElHassouny

ENSIAS, Mohammed V University in Rabat, Morocco

azeddine.elhassouny@ensias.um5.ac.ma

ABSTRACT

In most of the world's nations, groundwater management is infrequent despite its importance and scarcity. Continuous monitoring and precise projections of spatiotemporal groundwater recharge change can aid in sustainable development and effective groundwater resource management. Open public remote sensing datasets were used to develop machine learning prediction models (RF, XGBoost, AdaBoost, CatBoost, DT, Keras models) and time series forecasting models (CNN, LSTM, and its variants) for predicting and forecasting groundwater sheet recharge, respectively. The publicly available datasets are merged, processed, and organized into three parts for training, testing, and validation: 2002–2009, 2010–2015, and 2015–2020. A comparison of spatiotemporal prediction models' estimates of groundwater recharge in Morocco revealed that RF and XGBoost were the more accurate methods for temporal (spatial) recharging, with MAE values of 4.7795 mm/month (1.0227 mm/month) and 4.9936 mm/month (1.3031 mm/month), respectively. Regarding time series forecasting, the LSTM model performed better, with an MAE of 20.05 mm/month. The proposed models' performances on validation datasets demonstrate the utility and scalability of the proposed combined remote sensing and artificial intelligence-based framework, opening up a new pathway for large-scale groundwater management. The established workflow enables the study to be extended to any other site.

Index-words: *Groundwater recharge, Artificial intelligence, Remote sensing, Prediction, Forecasting, Time series, Tree vitality, Soil moisture.*

I. INTRODUCTION

GROUNDWATER is one of the most important sectoral exposures to climate change [1] and a vital component of maintaining the world's food supply. It is regarded as the primary source of fresh water and essential to preserving the planet ecological balance. Furthermore, it is a necessary component of the earth crust that prevents the earth from burning. Despite its significance and limited availability, it is hardly ever fully utilized and groundwater management is rarely done in most countries of the world [2].

The public release of official remote sensing data portals in recent years has broadened the range of applications for remote sensing analysis and boosted the size of the remote sensing community. Examples of these portals include those of the NASS [3], CHC-UCSB, OpenlandMap [4], and CSIRO. etc. With the increased availability of gridded hydrometeorological data and digitalized hydrography data with high spectral resolution for large scale, a variety of hydrologic applications may be precisely established for a country size.

Artificial intelligence (AI) has become more frequently incorporated into remote sensing-based groundwater management [5], offering innovative perspectives and new tools for predicting and forecasting groundwater behavior, including the status of groundwater supplies, groundwater levels and depth, recharge and withdrawal rates, and other hydrological variables [2], [6]–[10].

Data from remote sensing has been extensively analyzed using AI approaches for groundwater management. Machine learning (ML) including deep learning (DL) are algorithms that have the capacity to learn from vast amounts of data and produce predictions, forecasting, classifications, and so on. Support vector machines (SVM) [11], random forests (RF) [11], and artificial neural networks (ANN), among others, are examples of machine learning (ML) approaches that have been used to predict groundwater depth levels [12], [13], calculate recharge rates [14], and map groundwater potential zones [15].

For instance, the machine learning algorithm SVM is used to predict groundwater levels in the northeast United States using GRACE (Gravity Recovery and Climate Experiment), MODIS (Moderate Resolution Imaging Spectroradiometer), and in-situ climate variables [16]. Random Forests (RF) was used to forecast groundwater withdrawals in Arizona using publicly available datasets and in situ groundwater withdrawal data [2]. Regarding DL methods, groundwater management applications have used convolutional neural networks (CNN) and recurrent neural networks (RNN) to analyze remote sensing data to anticipate groundwater storage spatiotemporal change [17]. Convolutional neural network-LSTM (CNN-LSTM) and long short-term memory (LSTM) models were validated using on-site data from South Korea's National Groundwater Monitoring Network (NGMN).

Even though AI techniques have demonstrated significant potential for groundwater management based on remote sensing datasets, these techniques have only been tested in a few regions and countries, and there are still several challenges to overcome, including AI model interpretability, data availability, and data quality. Furthermore, more study is required to cope with the problem of fusing diverse data sources and producing more trustworthy AI models. The objective of this study is to investigate the fusing of hyperspectral multisource dataset perspectives and long-term forecasting, as well as predicting groundwater recharge/withdrawal in the feature space.

Groundwater is heavily used in agriculture in numerous Moroccan locations to grow year-round crops and trees such as watermelon, tomato, avocado, sours, oranges, and a variety of other specialty crops. Agriculture consumes 87% of water resources [18]. Morocco, like other parts of the world, has faced two major challenges over the last two decades: water- intensive agriculture and a dry climate with highly erratic precipitation. Reliable and accurate spatiotemporal groundwater recharge estimates are critical for determining the quantity of groundwater depleted and effectively managing groundwater resources. Groundwater fluctuations can be determined by hydrogeological features and boundary conditions of groundwater systems, as well as climatic, hydrological, and land cover change influences.

In this study, the authors establish a spatiotemporal groundwater recharge prediction and forecasting system (AI-GWR), which is, to their knowledge, a first of its kind. They estimate spatiotemporal changes in groundwater charges using remote sensing data and artificial intelligence. They develop an end-to-end workflow that starts with gathering datasets from multiple sources and moves on to preprocessing, fusing, scaling, normalizing, and other steps. The obtained dataset is based on several influencing factors, including meteorological, hydrological, soil moisture, and eva-transpiration data, as well as groundwater recharge information. In addition to using ensemble learning algorithms such as Random Forest (RF), AdaBoost, XGBoost, etc. To perform a prediction of GWR, investigate several CNN and RNN-based time series forecasting methodologies, such as LSTM, residual LSTM, and LSTM autoregressive. Before LSTM and CNN-driven windowing of datasets and the provision of a full deep analysis connected to target the groundwater recharge. Additionally, the authors carry out a more thorough investigation by formulating various data windowing strategies, such as temporal, spatial, and spatiotemporal. To validate the proposed approach, they conduct a novel case study of the Morocco region. They focus on how land use affects groundwater recharge in two areas in Morocco. For prediction and forecasting, they adapt cutting- edge algorithms.

The remaining portion of this work is structured as follows: the second section contains AI-based groundwater recharge estimations (AI-GWR). The study area and data processing are presented in Section III. Section VI provides an experimentation and discussion. The concluding section offers a perspective, a recommendation, and a conclusion.

II. AI-BASED-GROUNDWATER RECHARGE ESTIMATES (AI-GWR)

The AI-GWR's workflow is divided into many stages. As depicted in Fig. 1, it is divided into three major sections: Remote sensing Data Preparation-Thornthwaite-Mather (RSDP-TM) that consists of two parts (1) Data: Getting, preprocessing, and fusion (DGPF) and (2) TM procedure, and then (3) Artificial intelligence-based models (AIM).

The first step is to collect data from multiple sources, then prepare the dataset, and finally output and analyze. In the second block, in addition to several basic data processing operations, the authors fuse the prior block features files datasets. The datasets cover precipitation, evapotranspiration, hydraulic

characteristics, and groundwater recharge. The fusion operation entails combining all datasets into one and conducting any necessary operations to remedy issues such as interpolations, missing values, and so on. The obtained dataset includes all features for the specified date and location. The final block includes AI-based algorithmic operations like model fitting and evaluation. The entire pipeline is automated and relies on open-source or freely available programming languages, tools, and libraries. Tensorflow [19] with Keras [20] is used in this study to provide an approachable, highly- productive interface for solving machine learning problems, Python 3 [21] is used as the main programming backend for data acquisition, pre-processing, and implementing the machine learning model. The primary Python libraries used in the proposed workflow include NumPy [22], SciPy [23], scikit-learn [24], GeoPandas [25], Pandas [26], Folium [27], seaborn [28], matplotlib [29], xgboost [30]. QGIS [31] is used for statistical analysis and visualization.

A. Remote Sensing Data Preparation and Thornthwaite-Mather(TM) Procedure

1. Data: Getting, Preprocessing, and Fusion (DGPF)

The workflow is as follows: the authors use the Google Earth Engine platform to manage datasets from various sources [32], the TM method [33], [34] to provide spatiotemporal Groundwater recharge (GWR), and Tensorflow with Keras and Python 3-based libraries to build AI-based models.

The data collecting and pre-processing workflows are comparable to cutting-edge works [5], [35], [36]. The authors obtain Data from 2002 to 2020 using Google Earth Engine platform [32], [37] with the official data portals of NASA (MOD16A2.006: Terra Net Evapotranspiration(PET) 8-Day Global 500m), CHC-UCSB(The Climate Hazards Group Infrared Precipitation with Stations (CHIRPS) for Precipitation (Pr)) [38], OpenLandMap Soil Texture Class (USDA System), CSIRO(global plant root depth) datasets. Algorithm 1 includes a full description of each step.

In the case of groundwater recharge, OpenLandMap records are utilized to define the clay, sand, and organic carbon content of the soil. Hengl et al. [39] make available a global dataset of soil water content at field capacity with a resolution of 250 m. Now that the soil parameters have been specified, the water content at the field capacity and the wilting point was determined using the TM method (Section II-A2).

2. Thornthwaite-Mathe (TM) Algorithm [40]

Soil attributes datasets from OpenLandMap will be investigated. The wilting point and field capacity of the soil will be determined as hydraulic properties of soil by applying some mathematical formulas to a variety of image collections. After iterating through the meteorological image collection and hydraulic parameters of soil, the TM technique will be used to determine groundwater recharge in the area of interest.

- To relate water content at wilting point θ_{WP} to the soiltexture, Saxton and Rawls' equations [4] are utilized.

$$\theta_{WP} = \theta_{1500t} + (0.14\theta_{1500t} - 0.002) \quad (1)$$

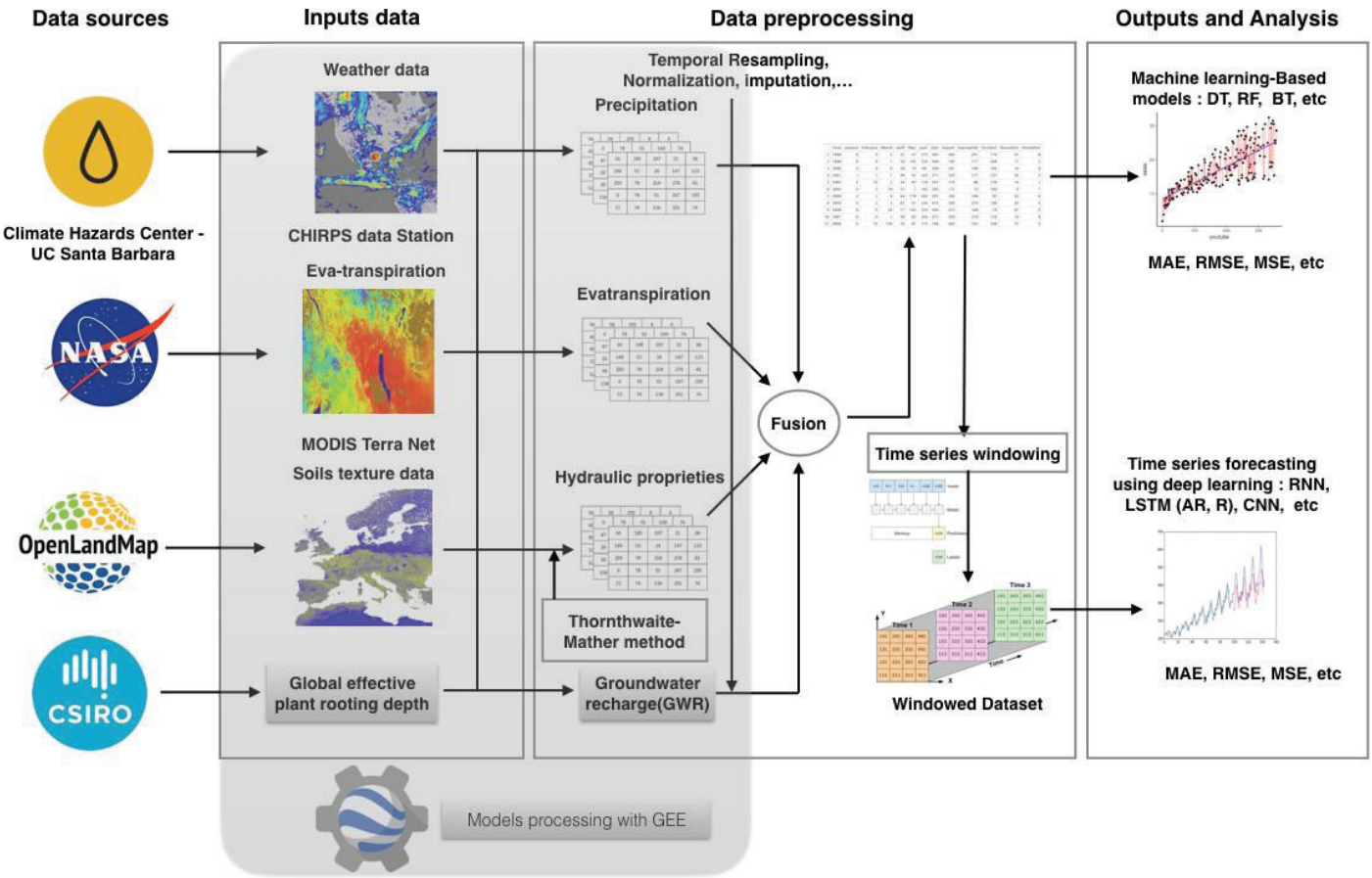

Fig. 1. Entire workflow, which includes downloading the input data and data preparation for generating predictor variables such as reprojection, resampling, statistical processes, and the Thornthwaite-Mather technique. The AI-based algorithmic stages are represented by the last block

with:

$$\theta_{1500t} = -0.024S + 0.487C + 0.006OM + 0.005(S \times OM) - 0.013(C \times OM) + 0.068(S \times C) + 0.031 \quad (2)$$

where: S: represents the sand content of the soil (mass percentage), $\mathcal{C}$: represents the clay content of the soil (mass percentage), and $\mathcal{OM}$: represents the organic matter content of the soil (mass percentage).

$$\mathcal{OM} = 1.724 \times \mathcal{OC} \quad (3)$$

- Similarly, the following formula is used to calculate the amount of water at field capacity :

$$\theta_{FC} = \theta_{33t} + (1.283\theta_{33t}^2 - 0.374\theta_{33t} - 0.15)w \quad (4)$$

with:

$$\theta_{33t} = -0.251S + 0.195C + 0.011OM + 0.006(S \times OM) - 0.027(C \times OM) + 0.452(S \times C) + 0.299 \quad (5)$$

For the TM process to be formalized, certain definitions are required. According to Allen [41], the following definitions are provided:

$$\mathcal{T}_{AW} = 1000 \times (\theta_{FC} \times \theta_{WP}) \times \mathcal{Z}_r \quad (6)$$

where: $\mathcal{T}_{AW}$: total soil water accessible in the rootzone, expressed in millimeters, θ_{FC}: the amount of water in the field when it is filled to capacity (m^3), and θ_{WP} refers to the water content at the wilting point (m^m)., $\mathcal{Z}_r$: rooting depth (in millimeters),

In Table 19 of Allen et al. [41] ,typical values of θ_{FC} and θ_{AW} for various soil types are provided.

The equation readily available water ($\mathcal{R}_{AW}$):

$$\mathcal{R}_{AW} = p \times \mathcal{T}_{AW} \quad (7)$$

where is $\mathcal{T}_{AW}$ total available water and p is the average percentage of total available water that can be exhausted from the root zone before moisture stress (between 0 and 1).

The preceding equations and steps are all combined in the TM algorithm 2.

Given the various AI algorithms for output prediction or forecasting, machine learning or deep learning, and different dimensions (temporal,

spatial, or spatiotemporal), the authors test ensemble learning and Keras models for spatiotemporal prediction, and CNN and LSTM for time series forecasting.

3. Machine Learning-based Spatiotemporal Groundwater Recharge Prediction (ML-GWR-STP)

When building a regressor model on a standard-form dataset, the most basic strategy is to utilize machine learning algorithms such as ensemble learning or any deep learning model to predict the value of a target variable (such as GWR) based on the values of the current predictor variables. The objective here is to accurately predict spatiotemporal groundwater recharge (GWR) using a variety of features. Some of the recently developed algorithms used to tackle similar problems are XGBoost, [42]–[44], and

Algorithm 1 DGPF Algorithm

Input:

i_{date}, f_{date}; //Initial and final dates of interest.
$\mathcal{P}_{oi}(L_{POI}, l_{POI})$; // Longitude and latitude that defines the location of interest with a point.
$\mathcal{F}_{VB}$; // Van Bemmelen factor.
$Scale$; //A nominal scale in meters of the projection to work in [in meters].
$Source$; //Source of dataset.

Output:

$\mathcal{DF}_m^{\mathcal{P}_{OI}}$ //meteorological dataset as a DataFrame at the location of interest;

procedure DGPF
//Initialization
Compute the wilting point θ_{WP}; //based on θ_{1500t} using Eq. (1)
Compute the field capacity θ_{FC}; //based on θ_{33t} using Eq. (4)
$\mathcal{S} \leftarrow$ GSPF((OpenLandMap datasets, Scale, SP = 'Sand'))
$\mathcal{C} \leftarrow$ GSPF((OpenLandMap datasets, Scale, SP = 'Clay'))
$\mathcal{OC} \leftarrow$ GSPF((OpenLandMap datasets, Scale, SP = 'Orgc'))
Compute Organic Matter $\mathcal{OM}$; //based on Organic Carbon content $\mathcal{OC}$ using Eq. (3)
$\mathcal{P}r \leftarrow$ EE.IMAGECOLLECTION() (UCSB-CHG/CHIRPS/DAILY, i_{date}, f_{date}, $\mathcal{P}_{oi}$, SP='precipitation')
$\mathcal{P}et \leftarrow$ EE.IMAGECOLLECTION() (UCSB-CHG/CHIRPS/DAILY, i_{date}, f_{date},$\mathcal{P}_{oi}$,SP='evapotranspiration')
$\mathcal{P}r(month) \leftarrow$ SUMRESAMPLER() ($\mathcal{P}r$, freq=1,scale_factor='month',band_name='Precipitation')
$\mathcal{P}et(month) \leftarrow$ SUMRESAMPLER(($\mathcal{P}et$, freq = 1, scale_factor = 'month', band_name = 'evapotranspiration'))
$\mathcal{DF}_{wearher} \leftarrow$ FUSION(($\mathcal{P}r(month), \mathcal{P}et(month)$))
end procedure=0

Algorithm 2 TM Algorithm

Input:

i_{date}, f_{date} ; // Initial and final dates of interest.
$\mathcal{P}_{oi}(L_{POI}, l_{POI})$; // Longitude and latitude that defines the location of interest with a point.
$\mathcal{F}_{VB}$: // Van Bemmelen factor.
$\mathcal{Z}_r(\mathcal{P}_{oi}(L_{POI}, l_{POI}))$; // rooting depth around our region of interest.
$\surd$; //parameter constant according to Table 22 of Allen et al. (1998).

Output:

$\mathcal{R}_m$; //Monthly Recharge
$\mathcal{ST}_m, \mathcal{APWL}_m$; //Available/Amount of water stored in the root zone for the month m

procedure TM
//Initialization
Compute averaged value between reference depths of the water content at field capacity $mean(\theta_{WP}(b_i))$; //based on $\theta_{WP}(b_i)$
Compute averaged value between reference depths of the water content at wilting point $(\theta_{FC}(b_i))$; // based on θ_{FC}
Compute the theoretically available water $\mathcal{T}_{AW}$; // based on (θ_{FC}) and (θ_{WP}) using Eq. (6)
if $\mathcal{P}_{et} \notin \mathcal{P}\nabla$ **and** $\mathcal{APWL}_m = \mathcal{APWL}_{m-1}(\mathcal{PET} - \mathcal{P}\nabla)$ **then**
  $\mathcal{ST}_m \leftarrow \mathcal{ST}_{m-1} + (P_m - PET_m)$; //amount of water stored in the root zone for the month m
else if $\mathcal{ST}_m \notin \mathcal{ST}_{FC}$ **then**
  $\mathcal{R}_m \leftarrow \mathcal{ST}_m - ST_{FC} + P_m - PET_m$; // recharge
  $\mathcal{ST}_m = \mathcal{ST}_{FC}$; // the water stored at the end of the month becomes equal to water stored at field capacity
else if $\mathcal{ST}_m \in \mathcal{ST}_{FC}$ **then**
  $\mathcal{APWL}_m \leftarrow ST_{FC} \times \ln(ST_m/ST_{FC})$; // the accumulated potential water loss for the month m
  $\mathcal{ST}_m = \mathcal{ST}_{FC}$; // and no percolation occurs
end if
end procedure=0

Volume 10, Issue 2, December 2024 - ISSN 2356-8569
http://dx.doi.org/10.21622/RESD.2024.10.2.933

Random Forest (RF) [2], [9]. To the authors' knowledge, prediction for groundwater recharge, storage, or withdrawals has only been done at this time using either current predictions [2], temporal updates [8], or distinct spatial and temporal updates. Hence, ensemble learning approaches like XGBoost, random forest (RF), etc., and the Keras model are examples that the authors use to address this issue.

4. Deep Learning-based Groundwater Recharge Time Series Forecasting (DL-GWR-F)

The purpose of multivariate or univariate groundwater recharge prediction is to anticipate present values in light of current or historical real-world conditions [2]. Groundwater recharge time series forecasting, on the other hand, focuses on predicting future values based on historical data. Modern sequence-to-sequence models use LSTM autoregressive across timesteps, which encourages temporal learning while ignoring evident spatial connections between variables, whereas CNN models directly reflect variable associations. However, these algorithms often undertake independent spatial and temporal updates and rely on established strategies that are immutable across time. In this study, the authors experimented with various AI-based time series forecasting algorithms such as LSTM, and CNN, with different strategies, including :

- **Univariate and Multivariate:** using one dependent variable which is recharge, or with other impacting factors such as precipitation, evaporation, etc.
- **Forecast for a single time step:** using a single feature, or all features.
- **Forecast multiple steps:** Single-shot that consists of mak- ing all predictions at once, or Autoregressive which makes one prediction at a time and feeds the output back to the model.

The main algorithm 3 summarizes the entire system and calls all functions.

Algorithm 3 Main Algorithm

Input:

$\mathcal{DF}_m^{\mathcal{P}_{OI}}$; //meteorological dataset as a DataFrame at the location of interest
$\mathcal{R}_m$; //Monthly Recharge
$\mathcal{ST}_m, \mathcal{APWL}_m$; // Available/Amount of water stored in the root zone for the month m
i_{date}, f_{date}; //Initial and final dates of interest.
$\mathcal{P}_{oi}(L_{POI}, l_{POI})$; // Longitude and latitude that defines the location of interest with a point.
$\mathcal{F}_{VB}$; // Van Bemmelen factor.
$Scale$; // A nominal scale in meters of the projection to work in [in meters].

Output:

$MSE, MAE, RMSE \cdots$; // all performance metrics

0: **procedure** MAIN
1: //Initialization
2: $\mathcal{DF}_m^{\mathcal{P}_{OI}} \leftarrow$ DGPF()(i_{date},f_{date},$\mathcal{P}_{oi}(L_{POI}, l_{POI})$,$\mathcal{F}_{VB}$, Scale,Source)
3: $\mathcal{R}_m, \mathcal{ST}_m, \mathcal{APWL}_m \leftarrow$ TM() (i_{date},f_{date},$\mathcal{P}_{oi}(L_{POI}$,$l_{POI})$, $\mathcal{F}_{VB}$, Scale, $\sqrt{}$, $\mathcal{Z}_r(\mathcal{P}_{oi}(L_{POI}, l_{POI}))$,Source)
4: $\mathcal{GDF}_m^{\mathcal{P}_{OI}} \leftarrow$ FUSION($(\mathcal{DF}_m^{\mathcal{P}_{OI}}, \mathcal{R}_m, \mathcal{ST}_m, \mathcal{APWL}_m)$);
5: $Reshape\ \mathcal{C}_m$; //based on T_i and C_i
6: $MSE, MAE, RMSE \leftarrow$ AIM($\mathcal{DF}_m^{\mathcal{P}_{OI}}, \mathcal{R}_m, \mathcal{ST}_m, \mathcal{APWL}_m$)
6: **end procedure**=0

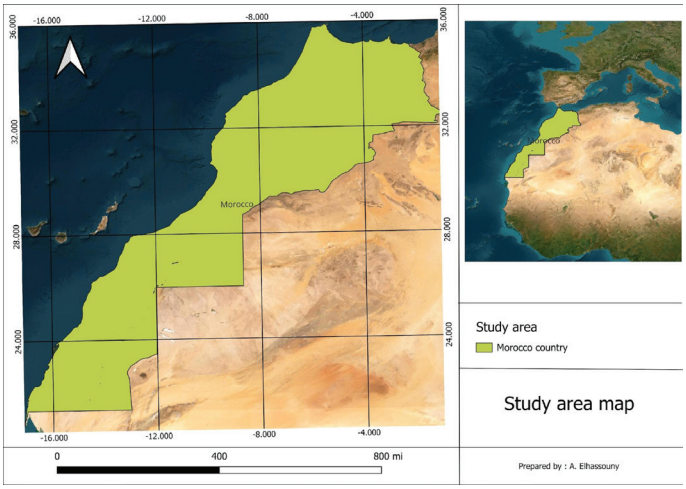

Fig. 2. Map of Morocco as the study area, as well as the Earth's largest hot desert, covering nearly all of northern Africa

III. STUDY AREA AND DATA

A. Study Area

The study area covers Morocco (Fig. 2) which is a sizable nation in north west Africa, stretching from the northern most point of the continent to the Sahel countries in its center. Its terrain and climate are diverse, with a total size of around 446,300 km^2. It lies between 20°00, 36°00*N* latitudes, and –18°00, –2°00*E* as longitudes. The nation has a tropical climate overall, with highs of up to 35°*C* (95°*F*) and lows of 5°*C* (41°*F*). In the Sahara regions have a hotter, drier continental climate, whereas the coast has a warm, moderate Mediterranean climate located on the north-west coast, which is influenced by south-easterly and north-westerly winds.

Several regions in Morocco heavily rely on groundwater for the year-round cultivation of crops and trees, including watermelon, tomato, avocado, sour cherries, oranges, and other specialty crops. Agriculture consumes 87% of water resources according to the High Commission for Planning (HCP) [18]. The authors use the whole Moroccan territory for a large-scale spatial prediction study area. Regarding time series data, the authors use monthly measurements from 2002 to 2020 from Taounate's two locations (Sidi Yahia Bni Zeroual and Ourtzagh) to forecast groundwater recharge (GWR) and train the LSTM and CNN-LSTM models. They choose two zones as test sites for evaluating their proposed strategy and hypotheses due to considerable discrepancies in crop output between the two zones, and reports of in situ groundwater depletion. Another rationale for selecting these locations was an understanding of the links between groundwater depletion for cannabis irrigation and tree vitality.

B. Data

Remote sensing–based data of characteristics that directly or indirectly affect groundwater recharge were used as input for machine learning models. For this investigation, the authors combine data such as meteorological, hydrological, etc, from numerous sources. The meteorological datasets consist of the following: MODIS Terra Net that provides evapotranspiration on an 8-day basis, and Climate Hazards Group InfraRed Precipitation with Station Data (CHIRPS) that provides precipitation daily, both of them with a resolution of 500 m^2.

Datasets from OpenLandMap are used to describe the amounts of clay, sand, and organic carbon in the soil. Hengl et al. [39] have made a global dataset of soil water content at the field capacity with a resolution of 250 m^2 available.

As a result, both parameters are determined in the following utilizing the global datasets that show the soil sand, clay, and organic matter contents together with the prior equations. As stated in the summary, in the TM method, the soil wilting point and field capacity are two hydraulic parameters that are frequently utilized. The wilting point denotes the depth beyond which plant roots cannot extract water, while the field capacity denotes the depth at which soil can no longer store water. Water seeps into the lower levels when gravitational pull exceeds a certain threshold. Allen's dataset [41] leads to the reasonable assumption that the effective rooting depth in the vicinity of the region of interest Taounate (Olive) is $\mathcal{Z}_r$ = 1.45.

The parameter *p* is likewise assumed to be constant and equal to p = 0.65, which is consistent with the typical values listed in Table 22 in [41], [45].

Input variables (Table I, Fig. 11) are adjusted using the z-score scaling method. This approach is defined by Eq. 8, which can be altered to limit the data range to a small range.

$$z = \frac{x - \mu}{\sigma} \tag{8}$$

TABLE I
DETAILS OF REMOTE SENSING DATASETS USED IN THIS STUDY.

Feature	Product	Dataset provider	Resolution	period	Description
Precipitation	CHIRPS	UCSB/CHG	0.05°,	1981-2023	Climate Hazards Group InfraRed Precipitation
Temperature	GLDAS-2.1	NASA GES DISC	0.25° × 0.25°	2000-2024	Global Land Data As similation System
Evaporization	GLDAS-2.1	NASA GES DISC	0.25° × 0.25°	2000-2024	Global Land Data As similation System
SM	GLDAS-2.1	NASA GES DISC	0.25° × 0.25°	2000-2024	Global Land Data As similation System
GWR	GWR	TM procedure of SM		2000-2024	Mean groundwater recharge

SM : Soil Moisture, TM: Thornthwaite-Mather

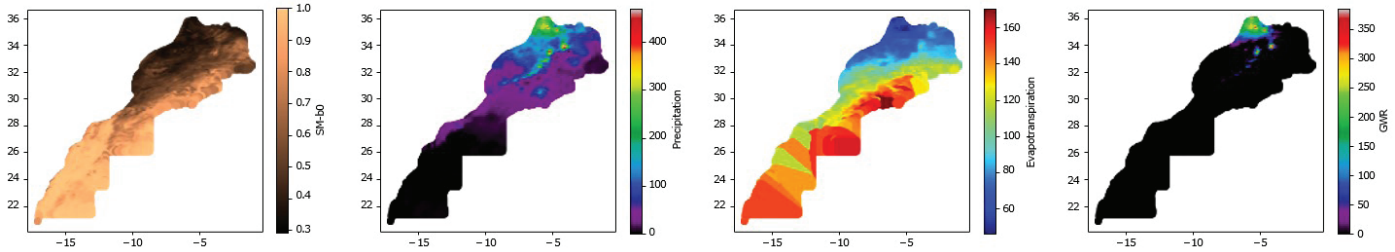

Fig. 3. Features maps: SM, precipitation, temperature, and GWR

IV. EXPERIMENTATION AND DISCUSSION

In this study, the authors successfully advance recent state- of-the-art works such as [2], [9], and extend the prediction of current groundwater recharge to forecast the future recharge of a new region by offering new insights and new methods, especially on using univariate and multivariate, forecasting future based on the past with different windowing, they also establish a pipeline to expand the application of their approach to any new region and relate the groundwater flow from mountains, trees vitality, and groundwater availability to the anticipated groundwater recharge and withdrawals. Finally, they suitably illustrate the extensibility of their approach to a framework, taking into account the fact that the used data are available for any region in the world.

a. ***Machine Characteristics:*** The experiment was conducted on a machine with the following specifications: 11th Gen Intel(R) Core(TM) i5-1135G7 processor with 2.40*GHz* x 2.42*GHz* and 8.00*GB* of RAM.

b. ***Training Paradigm:*** The authors employe two ways for data splitting. First, they divide the dataset into three sections: training, testing, and validation, with percentages of 50%, 25%, and 25%, respectively. They set up and loop the pipeline for numerous iterations to conduct all necessary tasks such as data preparation, feature engineering, model building, optimization, hyperparameter tuning, and validation. Second, they replicate the data for the second time, dividing it into two parts training and testing, with 50% and 50% respectively. They train the obtained models using ideal parameters obtained the first time, and then they test them on the testing part as depicted in Fig. 4.

c. ***Performance Metrics:*** For spatiotemporal prediction, the authors use a range of metrics [46], such as root mean square error (RMSE), mean square error (MSE), and mean absolute error (MAE). Apart from the previously mentioned metrics, time series forecasting employs additional metrics such as the persistency index (PI), squared Pearson's correlation coefficient (R2), relative root mean squared errors (rRMSE), absolute and relative biases (Bias and rBias), and the Nash-Sutcliffe efficiency (NSE) to evaluate forecast accuracy.

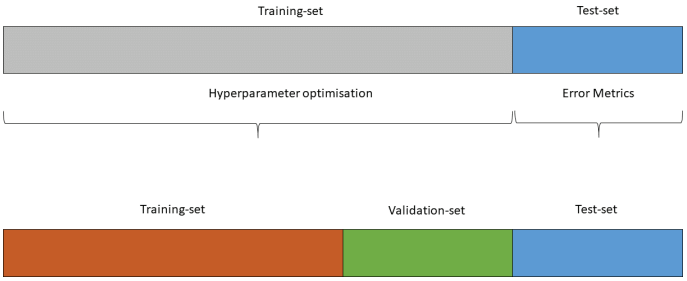

Fig. 4. Dataset is divided into three sections for training, validation, and testing

A. Machine Learning-based Spatiotemporal Groundwater Recharge Prediction (ML-GWR-STP)

The most straightforward model one can build on a dataset with a standard shape using XGBoost, Random Forest, or any other machine learning algorithms, predicts the value of a target variable, like GWD, based only on the values of the current predictor variables.

Fig. 5 illustrates the fact that the expected Groundwater recharge (GWR) for both the training period (2002–2013) and the validation period (2013–2020) is rather accurate. The authors built models such as RF (red line) and XGBoost (yellow line) can capture the temporal variations precisely. Here, the authors present just two models to avoid curve balding. However, one can notice that the RF model does not adequately capture the temporal patterns for the peak values low or high. This may be due to the hyperparameters max depth and min samples leaf, which control model overfitting. That conclusion is supported by the performance metrics mean absolute error (MAE) values of both models RF and XGBoost, which are 4.7795 *mm/month* and 4.9936 *mm/month*, respectively. As a result, the RF model outperforms all other models as depicted in table II. The MAE for deep learning-based models (Keras model) is approximately 7.2255 *mm/month*, which is still far from the precision obtained by ensemble learning techniques as indicated in the table II. Fig. 6 confirms the outcome. The precise groundwater recharge estimations for the test or validation data continue to demonstrate the model significant generalizability. The Random forest feature importance for Pr, pet, apwl, and st is 0.60, 0.063, 0.15, and 0.18, respectively, whereas for XGBoost it is 0.62, 0.047, 0.34, and $6.98e^{-08}$, in that order. The features importance demonstrates that recharge is primarily dependent on the amount of precipitation; the more precipitation, the more recharge. This is logical because, in the absence of precipitation, there is no water available for recharge or plant consumption, regardless of whether evapotranspiration occurs or not.

The normalized residual histograms in Fig. 7 a) show that the residuals are slightly left-skewed but closely reflect a normal distribution. In the same spirit, residual scatter plots with no discernible trend and residuals that are concentrated around 0 are shown in Fig. 7 c) and d) for both the RF and XGBoost models. As Fig. 7 b) further demonstrates, this implies that the residuals are independent and nearly normally distributed. Despite the slight bias, 98.48% of the standardized residuals of the XGBoost model reside in the [−2, 2] interval, indicating that its predictions are extremely robust. On the other hand, although RF achieves better MAE error performance than XGBoost, its standardized residuals fall within the [−25, 25] range. That conclusion is supported by Fig. 7 e) and f), which show that the regression scatters between the actual and predicted GWR by XGBoost follows a 1 : 1 relationship (Fig. 7 e)) but is very large for RF (Fig. 7 f)).

Compared to temporal predictions, the spatial predictions obtained by machine learning models are much more accurate as depicted in Fig. 8 and 9. Table III shows that the MAE metric is between 1.3031 *mm/month* by XGBoost and 0.7330 *mm/month* using the Keras model. This result makes sense considering that there are only minor variations in the roughly same features and output in a given location over a month. The large value of MAE gotten by the AdaBoost model (7.7255 *mm/month*) may be due to the hyperparameters tuning which leads to overfitting. The low values of all performance measures are caused by the fact that both the actual and predicted GWR values have many null values(zeros), which increases the divisor and lowers the mean value.

Fig. 10 depicts the residual analysis of the model estimates.

http://dx.doi.org/10.21622/RESD.2024.10.2.933

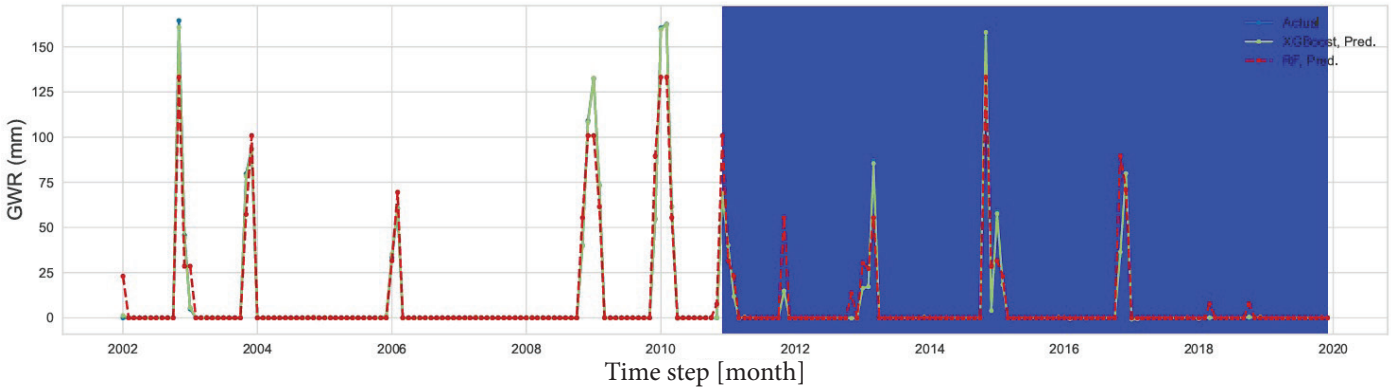

Fig. 5. Mean actual, XGBoost, and RF-based predicted groundwater recharge (GWR) over the region for each month, with 2010–2020 being the validation years

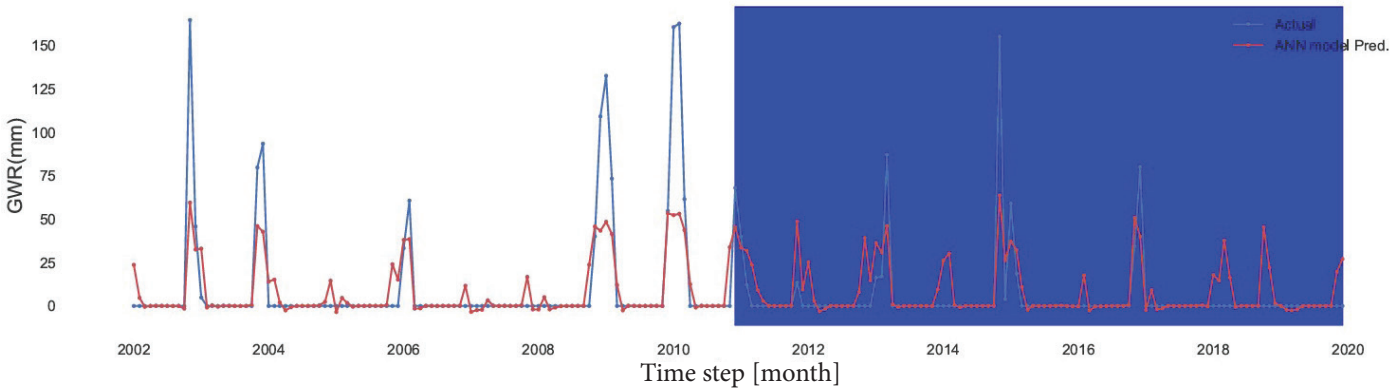

Fig. 6. Mean actual and Keras model predicted groundwater recharge (GWR) over the region for each month, with 2010–2020 being the validation years

TABLE II
TEST ERROR METRICS OBTAINED USING DIFFERENT MACHINE LEARNING MODELS-BASED TEMPORAL PREDICTION.

Model	MAE	MSE	RMSE	R2	RMSLE	MAPE	TT (Sec)
Random Forest Regressor(RF)	4.7795	190.6882	11.1021	0.4412	0.5401	nan	0.0500
AdaBoost Regressor(ADA)	4.5949	203.1542	10.9712	0.7540	0.4014	nan	0.8030
CatBoost Regressor(CATBOOST)	4.8592	162.9859	10.7098	0.4595	0.6233	nan	0.4840
Extreme Gradient Boosting(XGBOOST)	4.9936	212.4883	11.7745	0.3886	0.5507	nan	0.0160
Decision Tree Regressor(DT)	5.6609	299.4790	13.9545	0.5924	0.3698	nan	0.0080
Keras Model	7.2255	274.8504	16.5786	0.4685	Nan	1.8265	1.00

Volume 10, Issue 2, December 2024 - ISSN 2356-8569
http://dx.doi.org/10.21622/RESD.2024.10.2.933

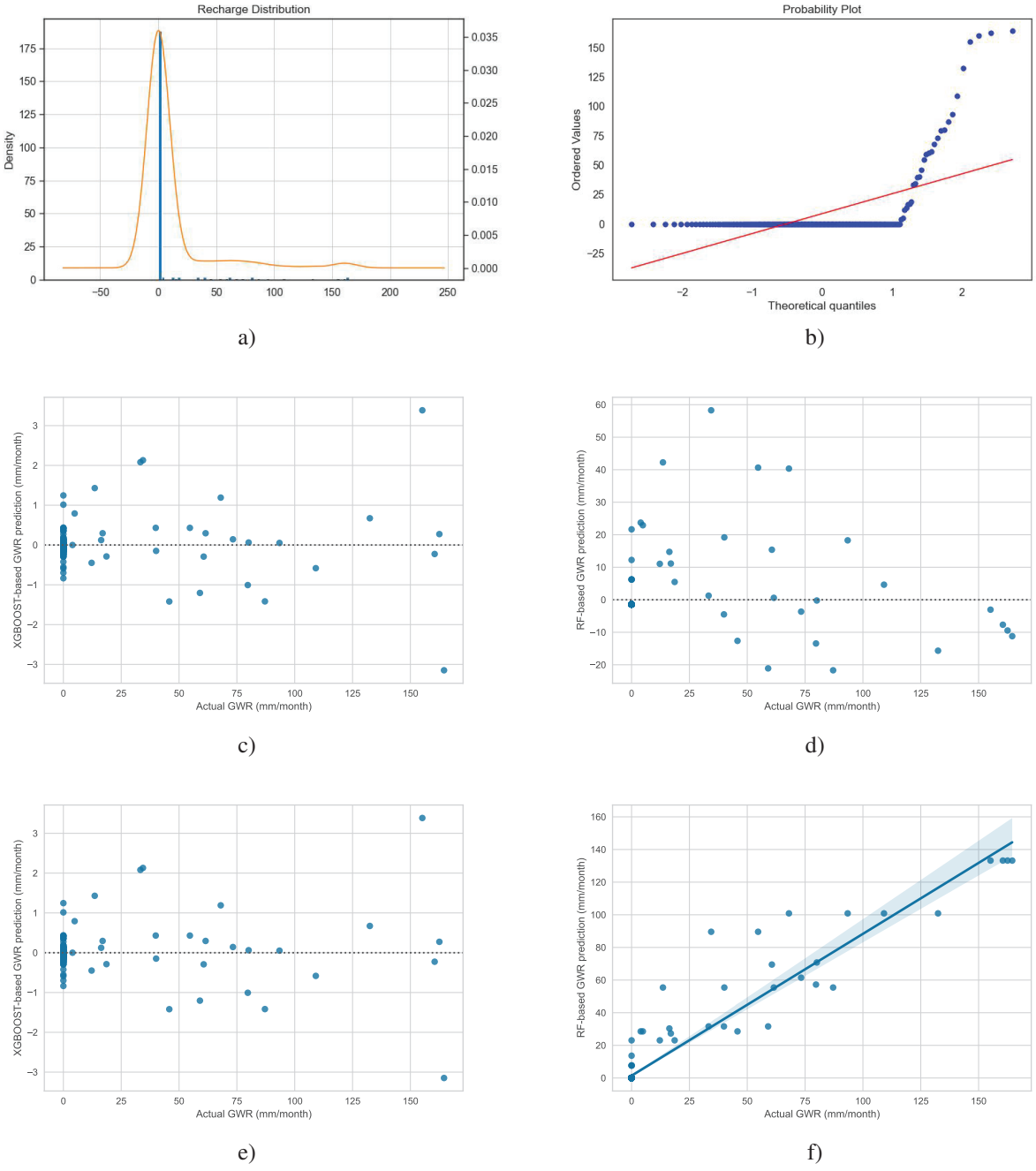

Fig. 7. Standardized residuals are restricted within the [−2,2] interval and Q–Q plots. Residual diagnostics (actual-predicted) for thegroundwater recharge (GWR) model RF and Keras model, respectively, representing the best and worst predictions for the test data (2013–2020). Scatter plot of the actual and predicted values For the best prediction model XGBoost and worst prediction RF of groundwater recharge (GWR)

Volume 10, Issue 2, December 2024 - ISSN 2356-8569
http://dx.doi.org/10.21622/RESD.2024.10.2.933

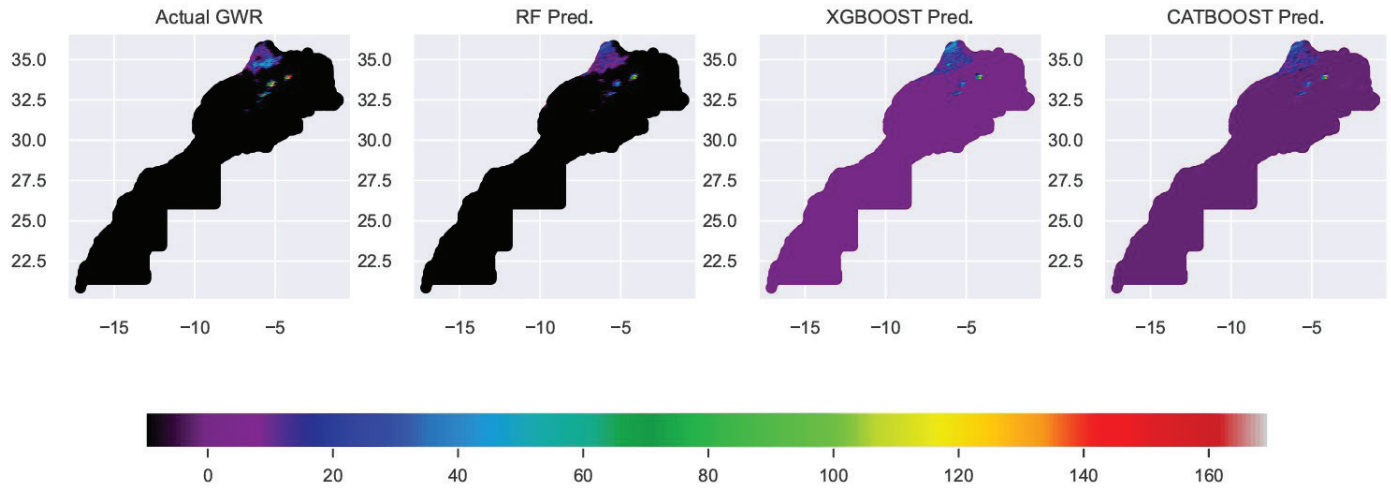

Fig. 8. Mean actual, machine learning models (XGBoost, RF, CatBoost)-based spatial predicted groundwater recharge (GWR) over the whole of Morocco

TABLE III
TEST ERROR METRICS OBTAINED USING DIFFERENT MACHINE LEARNING MODELS-BASED SPATIAL PREDICTION.

Model	MAE	MSE	RMSE	R2	RMSLE	MAPE	TT (Sec)
Random Forest Regressor(RF)	1.0227	26.5472	5.0089	0.9828	0.2274	0.7767	0.2060
CatBoost Regressor(catboost)	1.2154	31.0845	5.4822	0.9798	0.2779	0.8594	0.9720
Extreme Gradient Boosting(xgboost)	1.3031	42.2660	6.3056	0.9725	0.2703	0.7446	0.0420
Decision Tree Regressor(DT)	1.2542	46.7057	6.6822	0.9696	0.2269	0.7885	0.0130
AdaBoost Regressor(ADA)	7.7255	103.9699	10.0736	0.9316	1.8740	2.6578	0.9720
KerasModel	0.7330	9.0798	3.0132	0.8288	Nan	10.3525	0.986

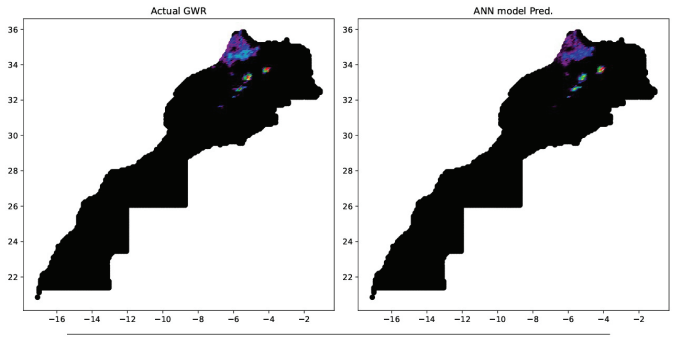

Fig. 9. Mean actual, Keras model-based spatial predicted groundwater recharge (GWR) over the whole of Morocco

Fig. 10. a) and b) demonstrate that in relevant recharge areas, models underpredict (negative mean error) more than they overpredict, and the majority of these huge errors occur in the extreme west-north and the chain of mountains of Atlas areas. In contrast, in the middle and south of Morocco, where the climate is extremely arid, with annual average precipitation rates nearing 0 *mm/year* in most places where no recharge occurs, the model predictions are close to the ground truth. Fig. 10. c) and d) depict residual scatter plots for both models, revealing no discernable features and residuals concentrated near 0. This indicates that the residuals are nearly normally distributed and independent. The standardized residuals for both models are in the large interval, which leads to worse forecasts. This is because of the issue with the picks predictions, as Fig. 10. e) and f) illustrate.

Volume 10, Issue 2, December 2024 - ISSN 2356-8569
http://dx.doi.org/10.21622/RESD.2024.10.2.933

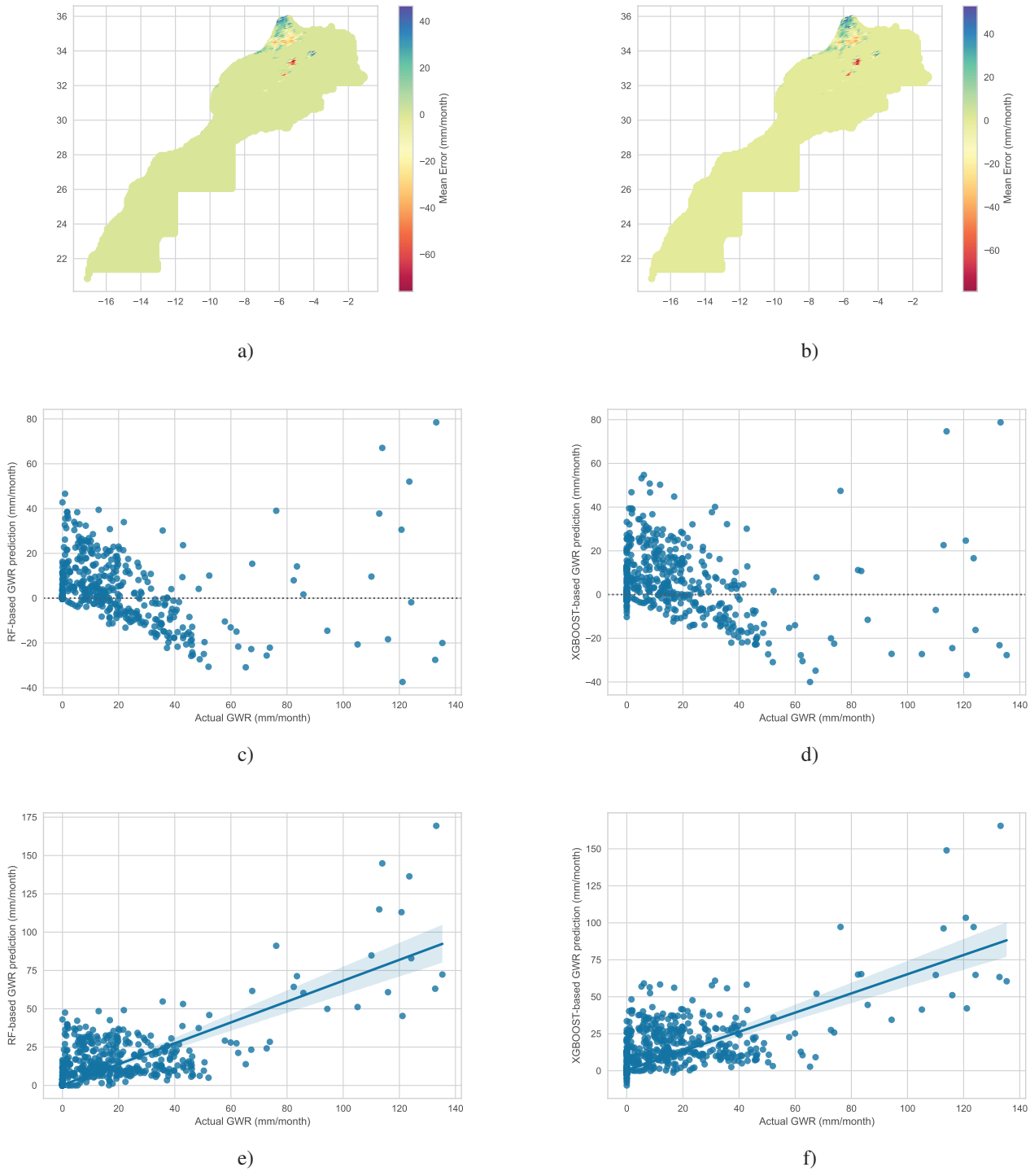

Fig. 10. The spatial distribution of the MSE between machine learning model-predicted GWR and interpolated in situ data throughout the testing period (January 2016). Residual diagnostics (actual-predicted) for the groundwater recharge (GWR) models RF and XGBoost, which indicate the best and worst predictions based on test data. A scatter plot comparing actual and expected values

B. Deep Learning-based Groundwater Recharge Time Series Forecasting (DL-GWR-F)

In this study, the authors extend machine learning-based models to deep learning-based models for time series forecasting. They investigate two advanced deep learning algorithms: Convolutional Neural Networks (CNN) and Recurrent Neural Networks (RNN)-based architecture, Long short-term memory (LSTM) in residual and autoregressive forms, with varied dataset windowing shapes, one last step to forecast one future step, many past steps to forecast one future step, many past steps to forecast many future steps. The main goal of this work is to forecast

Volume 10, Issue 2, December 2024 - ISSN 2356-8569
http://dx.doi.org/10.21622/RESD.2024.10.2.933

GWR in a given location. In this section's exploration part, the authors investigate the GWR variable and other features of the dataset to state hypotheses.

Fig. 11 depicts the evolution of all features such as precipitation (pr), evapotranspiration (pet), water lost in the field (apwl), water storage (st), and GWR (rech) over time from 2002 to 2020. They illustrate the evolution of characteristics over time to create periodicity hypotheses for time series- based algorithms. Also, Fig. 11 shows that there are not many disruptions, which is normal for natural occurrences. Fig. 12 illustrates the average GWR resampled over Month, Quarter, and Year for exploration purposes in order to identify the time unit of periodicity.

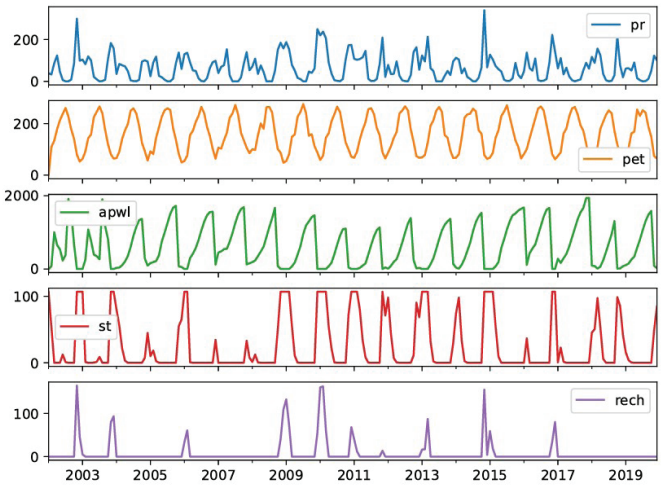

Fig. 11. Features maps: SM, precipitation, temperature, and GWR

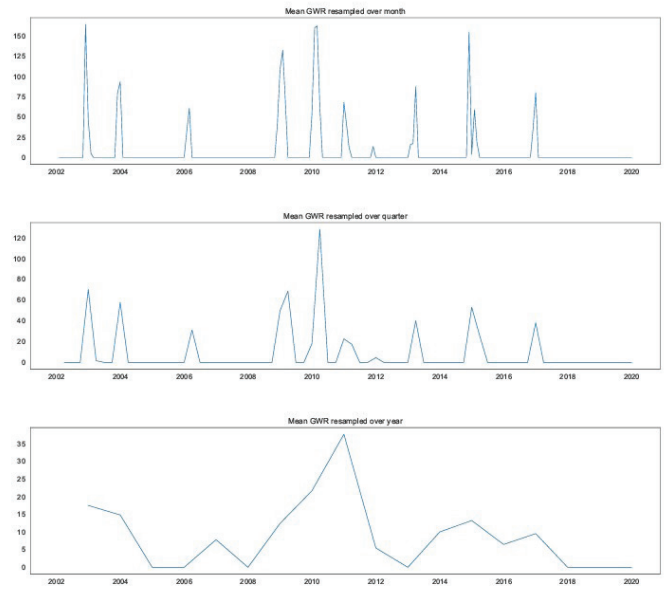

Fig. 12. Average GWR resampled over Month, Quarter, and Year

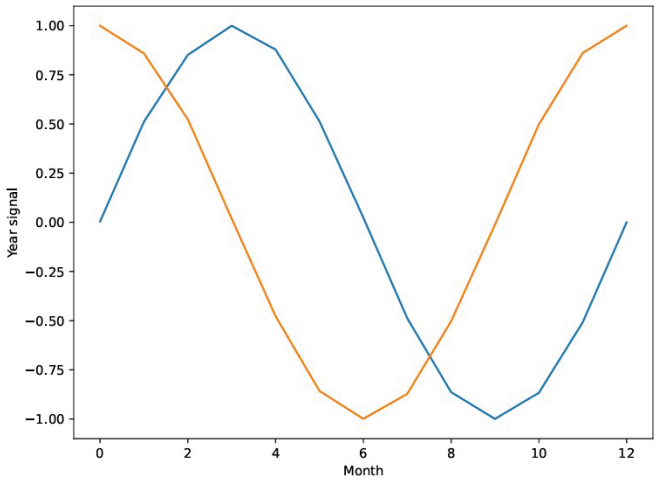

Fig. 13. Sine and cosine transform of GWR yearly signal $A_i^{(c)}$

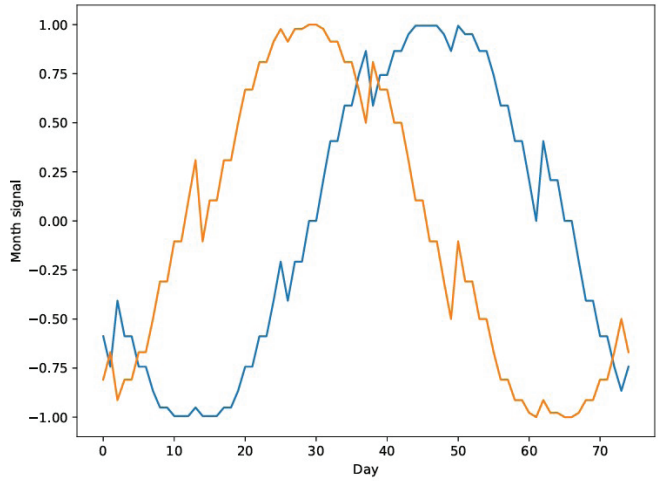

Fig. 14. Sine and cosine transform of GWR monthly signal $A_i^{(c)}$

There are numerous techniques to deal with periodicity. For example, sine and cosine transform can be used to figure out the time of season and year signals, making it possible to obtain acceptable signals. However, the time of day is not a suitable model input. Having data on groundwater recharge, it has a distinct quarterly and annual cycle, as shown in Fig. 13, 14.

The most crucial frequency features are accessible to the model through Fig. 13 and 14. In this instance, it is possible to understand the importance of time frequencies like year and season. For instance, by extracting features from the Fast Fourier Transform, one can figure out which frequencies are crucial. Fig. 15 shows that the noticeable peaks occur at a frequency close to $\frac{1}{\text{Year}}$.

Volume 10, Issue 2, December 2024 - ISSN 2356-8569
http://dx.doi.org/10.21622/RESD.2024.10.2.933

a. ***Data Windowing:*** There are four data windowing paradigms in the literature, One2One, One2Seq, Seq2One, and Seq2Seq [47], [48], and the choice of one of them is based on a hypothesis made upon many factors such as problem formulation, dataset shape, etc. However, a model that solely relies on the present circumstances to forecast the value of a single feature one-time step into the future. The current input values of a single-time-step model are unrelated to any previous values. It is unable to observe how the input features evolve over time. In order to handle the problem of forecasting Groundwater Recharge (GWR) based on predictors, the model requires access to numerous time steps for that reason the authors use Seq2One and Seq2Seq.

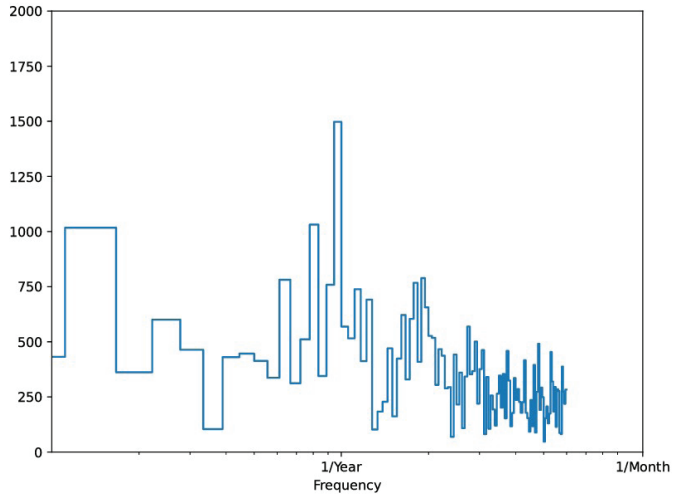

Fig. 15. Evolution of features overtime

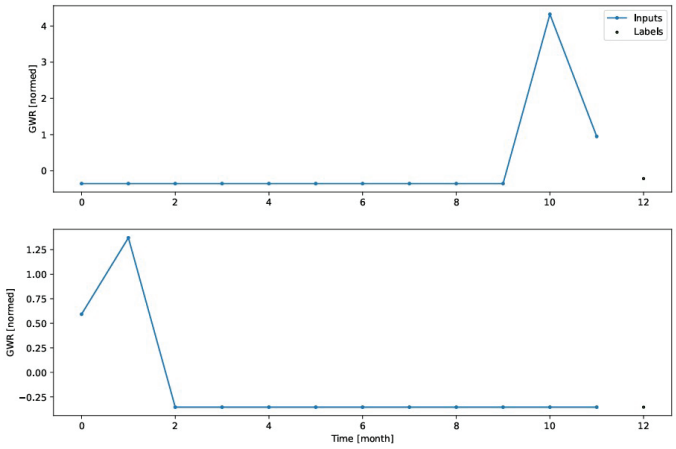

Fig. 16. Two examples of data windows of GWR variable with *Window(input = 12, labels = 1, shift = 1)*, GWR as feature and target variable in GWR univariate forecasting

To develop a model that can forecast future outputs based on the previous inputs, one needs to take a time series dataset which is a list of consecutive entries, and convert it into a window-shaped dataset of entries and label pairs (inputs, labels). Data windowing is a crucial stage in time series-based algorithms. One needs to specify the window(s) that determine the time step(s) in the past, time step(s) in the future, and offset time. Forecast one step at a time using all features or just one. To predict numerous phases at once, use single-shot forecasting. Make one prediction at a time with autoregressive, then feed the results back into the model. Data windowing is one of the primary pretreatments used to reshape data suitably for time series-based models. One may want to construct a variety of data windows depending on the task and type of model. To make a prediction one month into the future based on 12 months of history, for instance, one might define a window with *(input = 12, labels = 1, and offset = 1)*, alternatively, one could base a prediction 12 months into the future on one or several years of history, as indicated in the Figures 16, and 17).

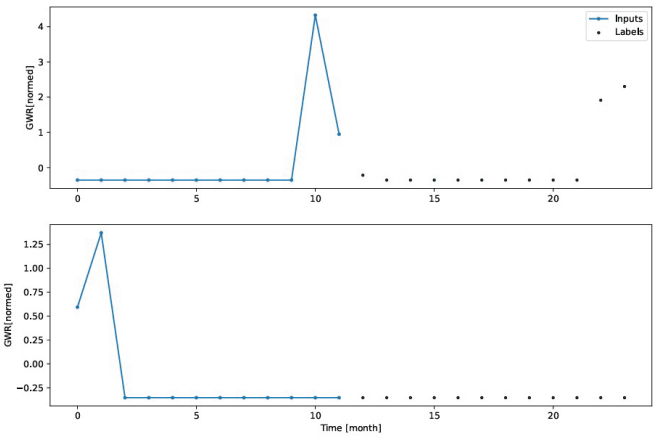

Fig. 17. Tow examples of data windows of GWR variable with *Window(input = 12, labels = 12, shift = 12)*, GWR as feature and target variable in GWR univariate forecasting

b. ***Univariate vs. Multivariate Forecasting:*** In terms of the features involved, there are two types: Univariate and multivariate forecasting. Univariate forecasting uses only one feature, in this case, the groundwater recharge (GWR) variable, whereas multivariate forecasting includes many features (more than two variables), including precipitation (pr),

Volume 10, Issue 2, December 2024 - ISSN 2356-8569
http://dx.doi.org/10.21622/RESD.2024.10.2.933

evapotranspiration (pet), water lost in the field (apwl), and water storage (st) features in addition to the GWR.

In a window with 12 timesteps of input and 12 timesteps of output, for the precipitation variable as well as other variables, one may only provide a series of timesteps of past values, for instance, 12 timesteps as shown in Fig. 18, but for the GWR variable, the authors provide 12 timesteps of past values and 12 timesteps as labels, resulting in 24 timesteps, as shown in Fig. 19. The 12 timesteps as labels are used to validate model predictions and calculate performance indicators.

1. CNN and LSTM-based Univariate GWR Forecasting

In this study, LSTM and CNN models powered by remote sensing data are built and evaluated. The models are built using TensorFlow, Keras, and Python 3. The LSTM model had an input layer, an output layer, a dense layer completely connected to hidden nodes, and an LSTM layer composed of each cell memory. Data are communicated through the max-pooling layer and flattened layer in the CNN model before being delivered from the input layer to the 2D convolution layer.

The authors build an LSTM model with 100 *neurons* in the first hidden layer and 1 *neurons* in the output layer to forecast groundwater recharge (GWR). The suggested model is assessed using the MSE loss function (Fig. 20), and the model is fitted with a batch size of 36 instances using the effective *Adam* version of stochastic gradient descent. The authors adjust several hyperparameters, including the number of training epochs, the dropout rate (20%), and the input shape, which will be many timesteps in the past to forecast one in the feature, depending on the forecasting window shape. Due to its ability to converge more quickly than the sigmoid or tangent hyperbolic functions, the ReLU function was chosen for use as an activation function.

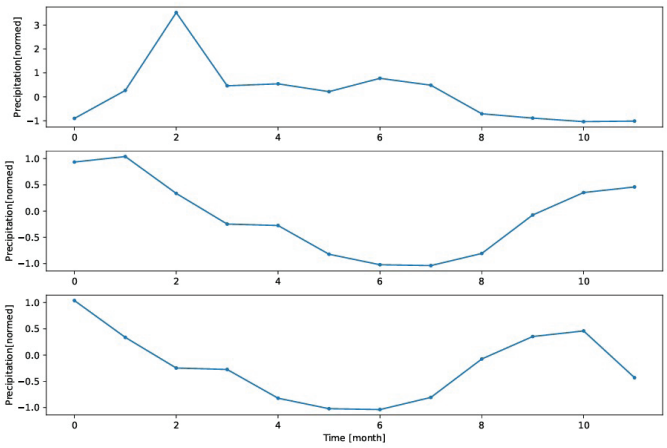

Fig. 18. Three examples of windows of precipitation feature with *Window(input = 12, labels = None, shift = None)*, as features in GWR multivariate forecasting

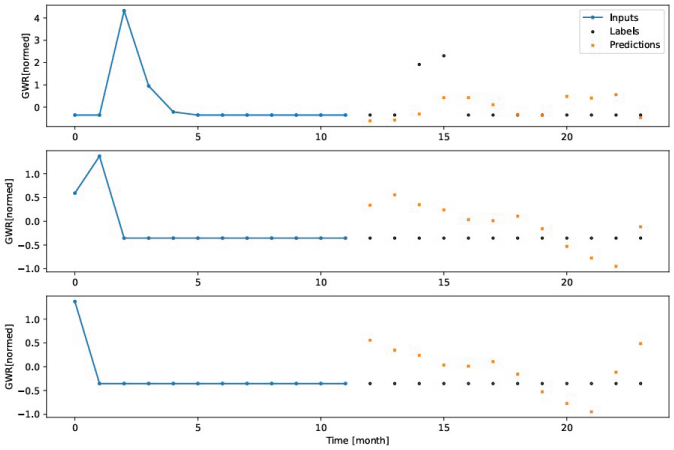

Fig. 19. Three examples of Data windows of GWR as feature and target variable with *Window(input = 12, labels = 12, shift = 12)*, in GWR multivariate forecasting

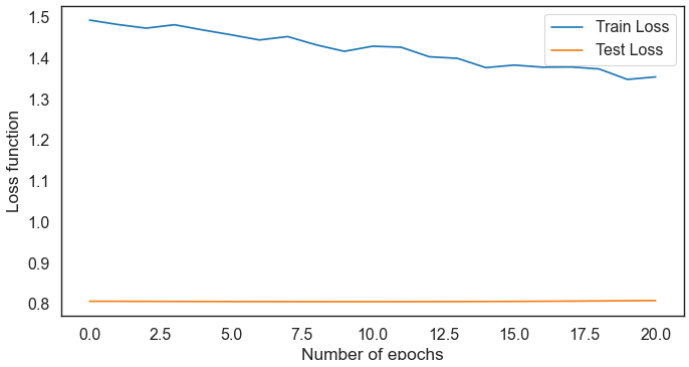

Fig. 20. LSTM Loss function changes according to the number of epochs for training and testing

Volume 10, Issue 2, December 2024 - ISSN 2356-8569
http://dx.doi.org/10.21622/RESD.2024.10.2.933

Deep learning models performance over Region of interest (ROI) is shown by the time series in Fig. 21. The magnitude and variability of GWRs obtained from the LSTM (red dotted line in Fig. 21) model were consistent with those of in situ measurements (blue line). The LSTM univariate model captured both the monthly and seasonal dynamics of in situ GWR, apart from showing stable performance for the test period (March 2013 to December 2019). However, a comparison of the LSTM model predictions with in situ measurements indicate that the model tends to underestimate large values while overestimating small or zero values of GWRs.

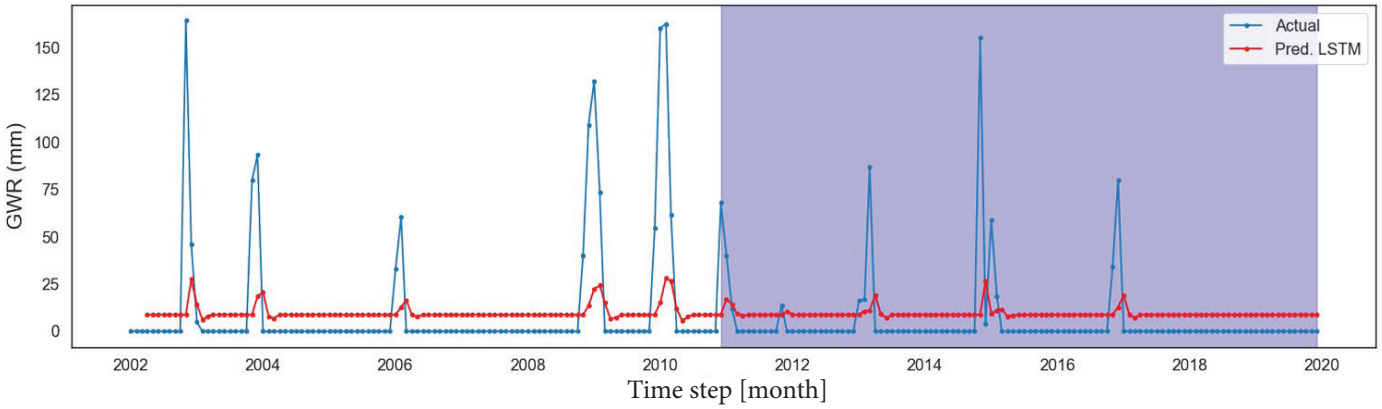

Fig. 21. GWR time-series comparisons predicted by the LSTM (red dotted line) Univariate model with in situ measurements (blue line)

2. LSTM and CNN-based Multivariate Forecasting

In the previous section, the authors attempt to forecast GWR based just on fluctuations in GWR, however, in this section, LSTM, and CNN models are utilized to accurately predict GWR over Morocco utilizing various feature combinations from multi-satellite data. The deep learning models include a variety of input variables (precipitation, evapotranspiration, changes in soil moisture storage, and so on). It is critical to understand the sensitivity of their predictive performance to avoid overfitting issues. The forecast accuracies of several parameter combinations are compared during hyperparameter optimization based on Bayesian optimization.

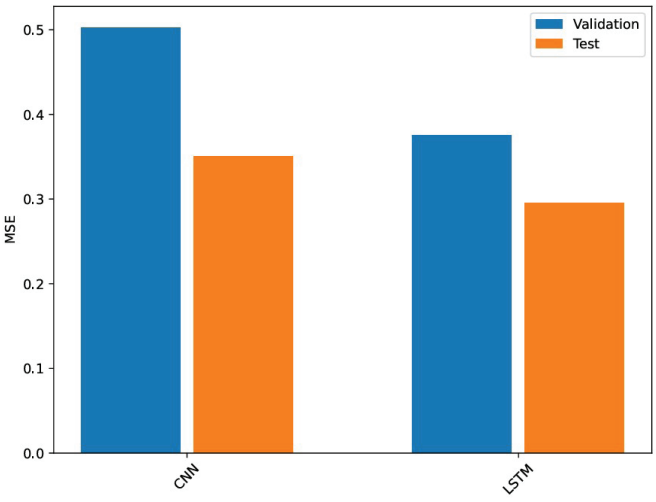

Fig. 22. Normalize RMSE error values for LSTM and CNN models for Test and Validation

a. ***Seq2One Multivariate LSTM, and CNN Forecasting:*** A comparison of the two deep learning models' predictions of groundwater storage change with in situ measurements of the GWR in Morocco revealed that the LSTM model is more accurate with Normalize RMSE (is determined using the normalized values of the true values and the anticipated values) RMSE = 0.2952 *mm/month*, than the CNN model with RMSE = 0.3501 *mm/month*. The outcomes are depicted in Fig. 22.

The deep learning models performance over ROI is shown by the time series in Fig. 23. The magnitude and variability of GWRs obtained from the LSTM (red dotted line in Fig. 23) and CNN (green line in Fig. 23) models are consistent with those of in situ measurements (blue line). The LSTM and CNN Multivariate models capture both the monthly and seasonal dynamics of in situ GWR associated with all features such as precipitation, evapotranspiration, APWL, ST, and recharge

Volume 10, Issue 2, December 2024 - ISSN 2356-8569
http://dx.doi.org/10.21622/RESD.2024.10.2.933

itself, apart from showing stable performance for the test period (March 2013 to December 2019). However, a comparison of the LSTM model predictions with in situ measurements indicates that the model tends to overestimate GWRs.

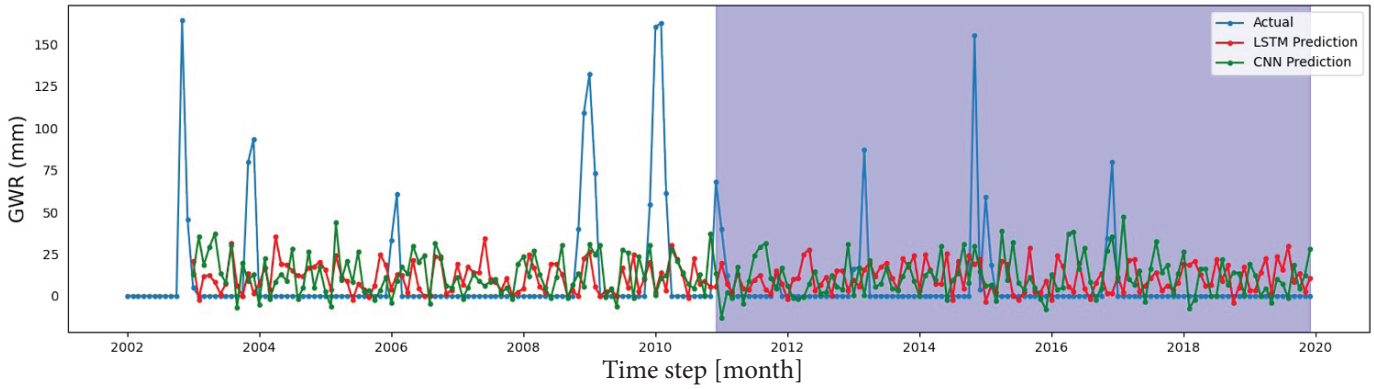

Fig. 23. GWR time-series comparisons Seq2One Multivariate forecasting by the LSTM, CNN Multivariate model with in situ measurements

b. ***LSTM Residual Model:*** Building models that forecast how the value changes in the following time step rather than the upcoming value is a typical practice in time series analysis. Similar to this, in deep learning, residual networks, or ResNets, refer to topologies where each layer increases the model cumulative output. That is how one benefits from the understanding that the change should be minimal. In essence, a model with a residual link facilitates faster convergence and somewhat improves performance. Any model can be utilized in conjunction with this strategy. The LSTM model, to which it is being applied in this instance, has been parametrized to make sure that the initially anticipated changes are modest and do not overwhelm the residual connection.

Fig. 24 illustrates how the residual technique outperformed LSTM in terms of forecasting, with RMSE falling from 0.4539 for the LSTM model to 0.4094 for Residual LSTM. With an RMSE of 0.3501, CNN remains the best model out of all those with and without residuals.

c. ***Seq2Seq Multivariate LSTM, CNN, and LSTM Autoregressive Forecasting:*** Both the single-output and multiple-output models in the previous sections made single-time step predictions, one month into the future. This section looks at how to expand these models to make multiple time-step predictions. In a multi-step prediction, the model needs to learn to predict a range of future values. Thus, unlike a single-step model, where only a single future point is predicted, a multi-step model predicts a sequence of future values. There are two rough approaches to this: (i) Single shot predictions where the entire time series is predicted at once. (ii) Autoregressive predictions where the model only makes single-step predictions and its output is fed back as its input. In this section, all the models predict all the features across all output time steps. For the multi-step model, the training data again consist of monthly samples. However, here, first, the models learn to predict 12 months (one year) into the future, given 12 months of the past (Fig. 25), and then to predict one year into the future, given 3 years of the past.

Autoregressive refers to that the output of each model can be fed back into itself at each stage, and predictions can be made based on the preceding one. The authors used both of the above models (CNN and LSTM) in an autoregressive feedback loop, but they build an LSTM-Autoregressive (LSTM-AR) model that is specifically designed for autoregressive feedback. Fig. 27 depicts the obtained result, which shows that LSTM-AR (sky blue line) captures well the change of GWR, after which CNN and LSTM executed an autoregressive feedback loop. The obtained RMSE for the three approaches are 0.4185, 0.4419, and 0.4590, in that order: LSTM-AR, CNN, and LSTM as shown in Fig. 26.

Volume 10, Issue 2, December 2024 - ISSN 2356-8569
http://dx.doi.org/10.21622/RESD.2024.10.2.933

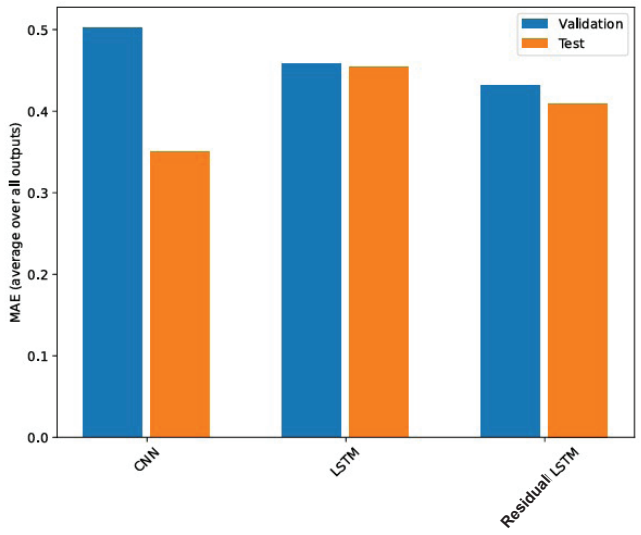

Fig. 24. Normalized RMSE error values for Residual LSTM, LSTM, and CNN models for test and validation

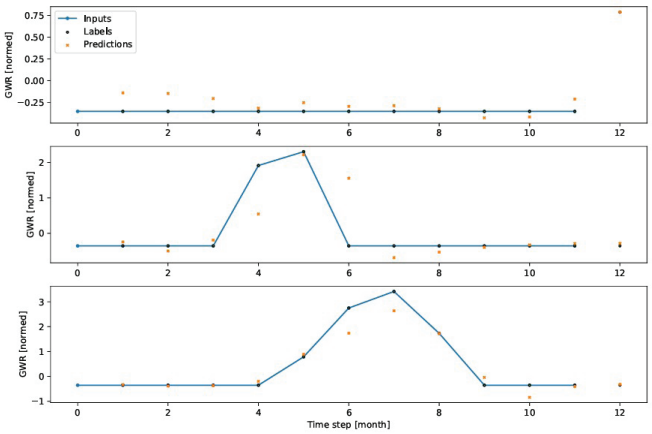

Fig. 25. Example of data windows of GWR variable with the blue dotted line as inputs, black dots as actual labels, and orange dots as forecasted values:
Window(input = 12, labels = 12, shift = 1)

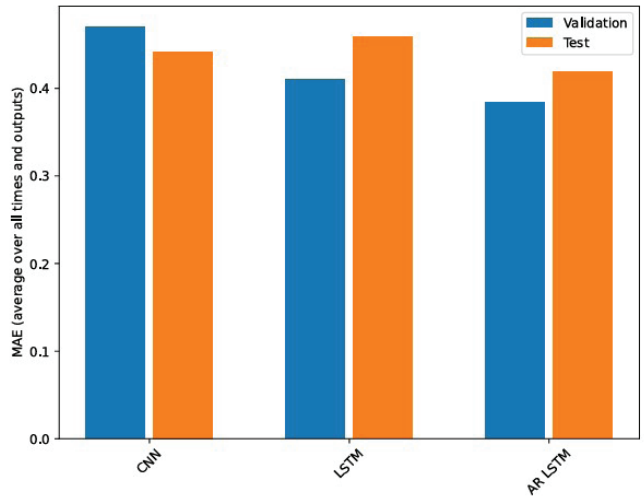

Fig. 26. Normalize RMSE error values for LSTM-Autoregressive (LSTM-AR), LSTM, and CNN models for Test and Validation

d. Long-term Autoregressive LSTM Forecast: Given the importance of long-term forecasting systems in general, and groundwater in particular, the authors anticipate a lengthy duration of investigation to pave the way for building lengthy-term memory by investigating autoregressive principles. For predicting the future value of GWR, the RMSE function is used following the number of time steps to be taken into account. One can learn about the best window shape for accurate prediction. Fig. 28 shows the plot showing the correlation between the RMSE and the number of history timesteps used to forecast the GWR value during the whole period. As seen in Fig. 28, the value of a window from which one obtains the minimum MSE is the three timesteps in a month. When they try to anticipate the far future, the MSE value rises; the further they go into the future, the more imprecision they receive.

The authors discovere that a good period in the past to predict one year in the features is three years after hyper-parameters tweaking with regard to the past period and future period. Figure 29 displays the predictions made using the LSTM autoregressive model and the ground truth of the GWR. More than any other model before it, the model accurately represents the high and low values in GWR. This conclusion is supported by Normalized MAE *RM AE* = 0.4815 as depicted in Fig. 28. As shown in Fig. 29, they investigate 3 years in the past to predict 1 year in the future.

It is well understood that groundwater recharge cannot be readily monitored and is influenced by spatially and temporally complicated processes. In addition, Groundwater is critical to the preservation of ecosystems and the adaptation of humanity to climate change which is with long-term impacts. However, given the importance of long-term forecasting systems in general, groundwater recharge, storage, and withdrawal in particular, and as shown in Fig. 30, the authors investigate the prospect of long-term future forecasting, which, while not precise, is a significant tool for capturing groundwater dynamics and providing scientific guidance for decision-makers.

Volume 10, Issue 2, December 2024 - ISSN 2356-8569
http://dx.doi.org/10.21622/RESD.2024.10.2.933

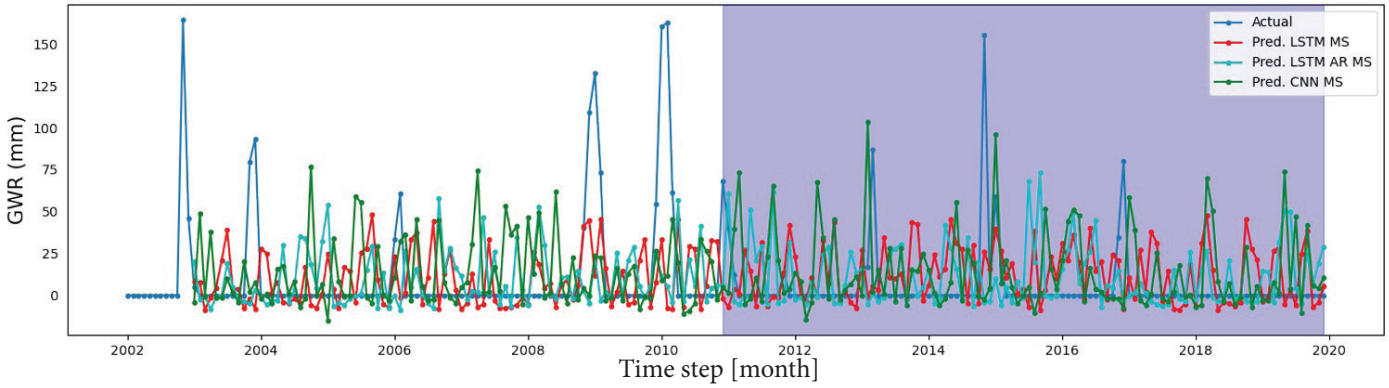

Fig. 27. GWR time-series comparisons Seq2One Multivariate forecasting by LSTM, LSTM AutoRegressive, CNN Multivariate models with in situ measurements

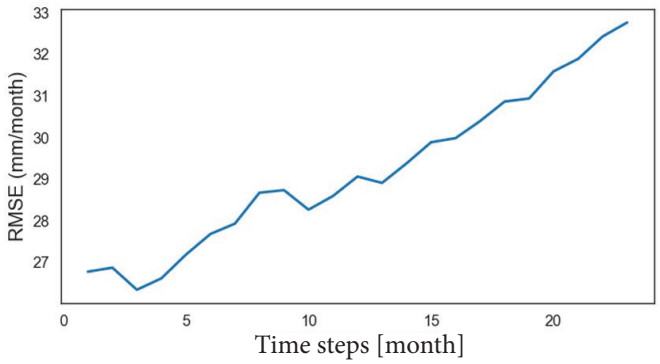

Fig. 28. RMSE according to the number of timesteps of the past to take into consideration to predict the future value of GWR

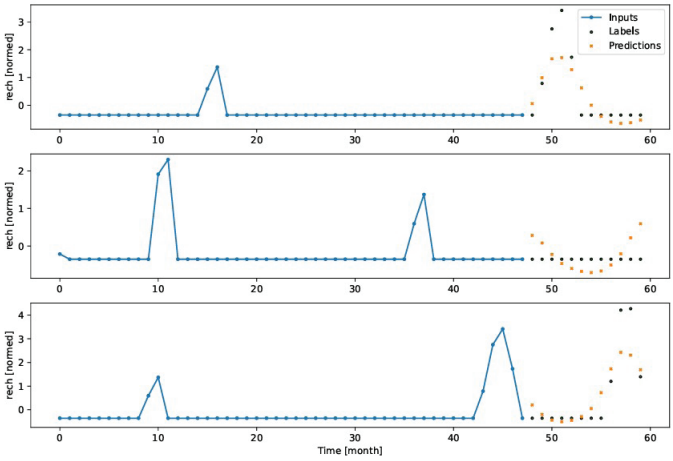

Fig. 29. Example of data windows of GWR variable, blue dotted line as inputs, black dots as actual labels, and orange dots as forecasted values:
Window(input = 36, labels = 12, shift = 1)

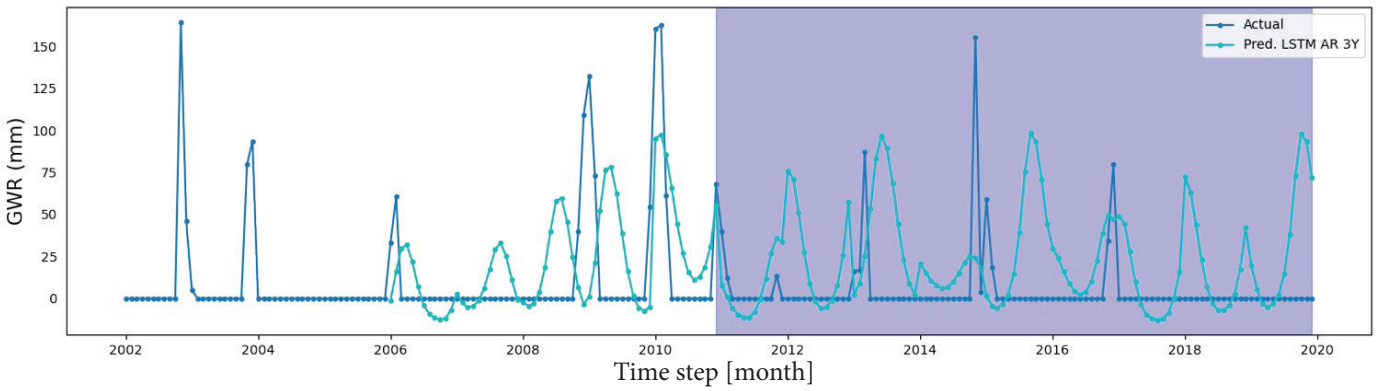

Fig. 30. Multivariate forecasting of one year (12 months) in the future based on 3 years in the past

Volume 10, Issue 2, December 2024 - ISSN 2356-8569
http://dx.doi.org/10.21622/RESD.2024.10.2.933

e. ***Hyperparameters Tuning:*** In this study, the hyperparameters tuning for the deep learning algorithms such as CNN, and LSTM are found using cross-validation using Bayesian optimization techniques based on Python's Keras tuning library. The optimization range of values and hyperparameter sets are set up as depicted in Table IV.

TABLE IV
HYPERPARAMETERS OF THE DEEP LEARNING MODELS AND THE OPTIMIZATION RANGE OF VALUES.

Model	Hyperparameter	Range of values
LSTM	Number of hidden layers	{1, 2, ⋯ , 10}
	Number of nodes per layer	{5, 10, ⋯ , 150}
	Time lag (month)	{1, 2, ⋯ , 12}
	Dropout rate	{0.1, 0.2, ⋯ , 0.5}
	Batch size	{16, 32, ⋯ , 128}
	Epoches	{1, 2, ⋯ , 100}
	Seq lenth	{1, 2, ⋯ , 52}
CNN	Number of filters	{16, 32 ⋯ , 128}
	Number of hidden layers	{1, 2, ⋯ , 10}
	Number of nodes per layer	{1, 10, ⋯ , 100}
	Time lag (month)	{1, 6, ⋯ , 12}
	Dropout rate	{0.1, 0.2, ⋯ , 0.5}
	Batch size	{5, 10, ⋯ , 128}
	Epoches	{1, 10, ⋯ , 100}
	Dense Size	{1, 2, ⋯ , 256}
	Seq length	{1, 2, ⋯ , 52}
	Number of filters	{1, 2, ⋯ , 256}

Table V shows the most performance measures for both techniques with tuned hyperparameters, which favor the LSTM technique over CNN.

TABLE V
TEST ERROR METRICS OBTAINED USING DIFFERENT AI-BASED ALGORITHMS WITH TUNED HYPERPARAMETERS.

Model	Error metric	Range of values
LSTM	NSE	−0.87
	R^2	0.10
	RMSE	20.05
	rRMSE	12.19
	Bias	15.13
	rBias	9.19
	PI	−0.43
CNN	NSE	0.05
	R^2	0.09
	RMSE	22.31
	rRMSE	13.56
	Bias	2.80
	rBias	1.70
	PI	−0.07

C. Hypothesis Validation with the in Situ Information

Fig. 31 displays the annual precipitation average in millimeters per year (mm/year), while Fig. 32 displays the annual recharge average in millimeters per year (mm/year). While recharge varies between 0 *mm/y* and 500 *mm/y*, precipitation rates range from 500 *mm/y* to 1500 *mm/y*. The blue dots in Fig. 31 indicate a rate of precipitation of about 900 *mm/year*; the authors observe consistency in Fig. 32, and the green points indicate a rate of recharge of about 300 *mm/year*, and so on for all points pairwise comparisons between Figures 31 and 32. One can observe that the rates of recharge (Fig. 32) and precipitation (Fig. 31) are completely correlated. Recharge increases in direct proportion to precipitation, and vice versa. This conclusion backs up the previous one that is reached using temporal data. One can infer from this that precipitation and recharge are spatially correlated. Consequently, there is a spatiotemporal regression between precipitation and recharging.

According to Fig. 33, Sidi Yahia Bni Zeroual's (place 1) annual recharge is approximately twice as high as Ourtzagh's (place 2). The outcome also demonstrates a high degree of yearly recharge variability, with values in places 1 and 2 ranging from 0 *mm/year* to 430 *mm/year* and 0 *mm/year* to 220 *mm/year*, respectively. The result also demonstrates that there has been no recharging in the two locations over the last three years. The authors observe during their visit to both locations that, despite the first location receiving more recharge due to its higher precipitation, the vitality of the trees has decreased and the habitats are suffering from thirst and well depletion, whereas the second location, despite receiving less recharge and precipitation, has healthy trees and wells that are still filled with water. Because of the changing climate, Morocco and the rest of the world are experiencing lower precipitation. Given the established spatiotemporal relationship between groundwater recharge and precipitation, one can conclude that groundwater

Volume 10, Issue 2, December 2024 - ISSN 2356-8569
http://dx.doi.org/10.21622/RESD.2024.10.2.933

is a limited resource, and uncontrolled depletion of this priceless substance poses a serious risk to the sustainability of life.

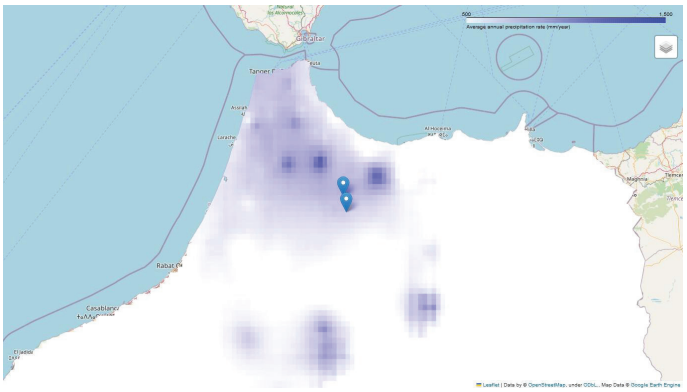

Fig. 31. Average annual of precipitation rates (*mm/year*), including two areas of study, in the north of Morocco

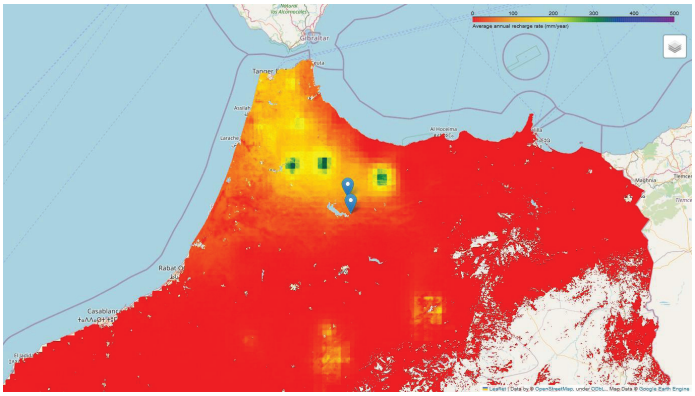

Fig. 32. Average annual of recharge rates (*mm/year*), including two areas of study, in the north of Morocco

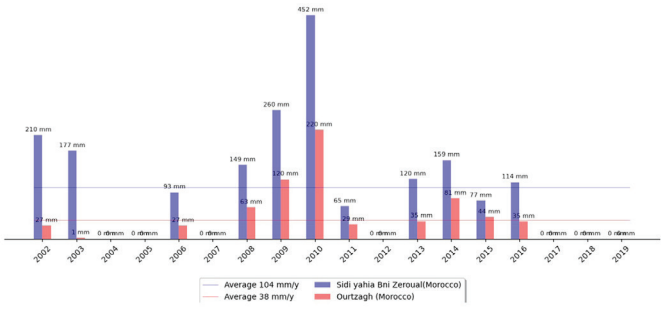

Fig. 33. Groundwater recharge comparison between the two places

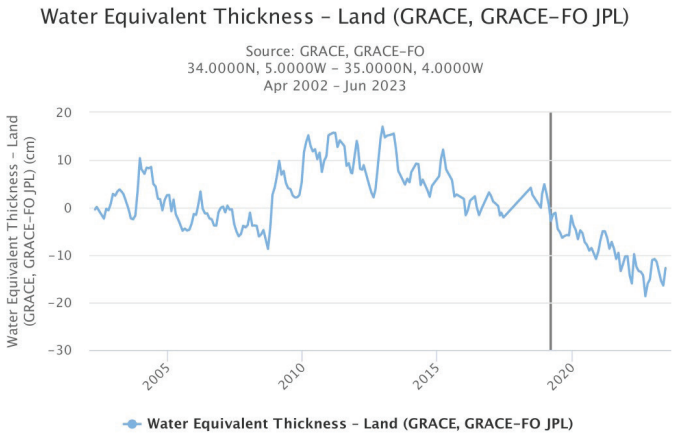

Fig. 34. Water equivalent thickness of place 1 (ROI1)

For areas dominated by Groundwater irrigation, as shown in Place 1, groundwater withdrawal causes a negative water equivalent thickness and drop in total water storage as shown in Fig. 34. It is evident that starting in 2019, the overall water storage has decreased below zero and has continued to decline significantly, even dropping.

The scenario is as follows, according to the data the authors have gathered from the locals of the area: Around 20 years ago, people used surface water for agriculture and the water came from mountains. Agriculture consisted of subsistence crops such as wheat, vegetables, and melons. Since the year 2000, residents of place 1 have switched from subsistence farming to cannabis farming, which is a spring-summer culture with little precipitation. Farmers began digging wells illegally and without authorization, and as people realized that each well meant a loss of a source of water flow from mountains, more wells were drilled until there was no longer a source of water flow from mountains. The locals began drinking water from wells. When the water in the wells first started to run out, they were around 60 meters deep. Farmers then dug new, deeper wells, and so on. More than 50 wells of various depths are now counted in the area of 6 km^2 in place 1. People in that area suffer from thirst, so the local authority brings drinking water pipes from another location because there are only two wells with a high deep depth and little water available in Place 1. Locals have informed the authors during their tour that many families had left the region and moved to large cities like Tanger, Fes, and Casablanca.

V. CONCLUSION, PERSPECTIVE, AND RECOMMENDATION

Physical modeling of the GWSC requires extensive data for numerous variables, and highly skilled researchers, and is a nonlinear and demanding undertaking. A viable alternative to traditional models for capturing complicated interactions between GWR-related factors is artificial intelligence (AI). Additionally, it is simple to include satellite data for multiple factors to forecast spatiotemporal GWR with AI models. In this study, several feature combinations from multi-satellite data are used to forecast GWR across Morocco accurately using CNN and LSTM models, including different variations of residual and autoregressive models. Different input variables (precipitation, average evapotranspiration, changes in soil moisture storage, AWPL, and ST) are used in the deep learning models. To prevent overfitting issues, it is important to comprehend the sensitivity of their predictive performance. Different parameter combinations are used for hyperparameter optimization based on Bayesian optimization, and the combinations prediction accuracies are compared. Overall, the findings demonstrate that, in terms of the RMSE, the LSTM autoregressive model predict GWR maps somewhat better than the other models described in this study.

As was previously noted, managing groundwater involves keeping track of various processes, including recharge, storage, withdrawal, depth level, etc. The first natural process is a recharge, in which freshwater seeps into the earth to restock subsurface aquifers. The other processes mentioned above follow and are the focus of the authors' following studies.

Active monitoring of groundwater recharge, storage, and withdrawals is still restricted to just a few places worldwide, despite the growing global drive toward sustainable groundwater management techniques and water security in general. In this work, the authors effectively illustrate the applicability and adaptability of their AI and remote sensing methods- based approach, which might help water managers achieve their goals for water management. In Morocco, agriculture is becoming increasingly reliant on irrigation, and while the authors recognize the importance of agriculture to the national economy and its value in providing food for ecosystems, rising withdrawal rates in unmanaged basins are dangerous and pose a threat to the national reserve.

Data Availability

The datasets generated during and/or analyzed during the current study are available online as described in the Data subsection, and in Fig. 1.

Acknowledgments

The authors would like to thank the Remote Sensing Frameworks for making datasets available to the public for free.

Competing interests

The authors declare no competing interests.

Ethical approval

This article does not contain any studies with human participants performed by any of the authors.

Informed consent

This article does not contain any studies with human participants performed by any of the authors. Since this article includes spatial analysis processes that do not require data collection from humans, consent was not required.

References

[1] S. A. Sarkodie, M. Y. Ahmed, and P. A. Owusu, "Global adaptation readiness and income mitigate sectoral climate change vulnerabilities," *Humanit Soc Sci Commun*, vol. 9, no. 1, 2022, doi: 10.1057/s41599-022-01130-7.

[2] S. Majumdar, R. Smith, B. D. Conway, and V. Lakshmi, "Advancing remote sensing and machine learning-driven frameworks for groundwater withdrawal estimation in Arizona: Linking land subsidence to groundwater withdrawals," in *Hydrological Processes*, 2022. doi: 10.1002/hyp.14757.

[3] G. B. Senay *et al.*, "Operational Evapotranspiration Mapping Using Remote Sensing and Weather Datasets: A New Parameterization for the SSEB Approach," *J Am Water Resour Assoc*, vol. 49, no. 3, 2013, doi: 10.1111/jawr.12057.

[4] K. E. Saxton and W. J. Rawls, "Soil Water Characteristic Estimates by Texture and Organic Matter for Hydrologic Solutions," *Soil Science Society of America Journal*, vol. 70, no. 5, 2006, doi: 10.2136/sssaj2005.0117.

[5] B. Janga, G. P. Asamani, Z. Sun, and N. Cristea, "A Review of Practical AI for Remote Sensing in Earth Sciences," 2023. doi: 10.3390/rs15164112.

[6] A. Wunsch, T. Liesch, and S. Broda, "Groundwater level forecasting with artificial neural networks: A comparison of long short-term memory (LSTM), convolutional neural networks (CNNs), and non-linear autoregressive networks with exogenous input (NARX)," *Hydrol Earth Syst Sci*, vol. 25, no. 3, 2021, doi: 10.5194/hess-25-1671-2021.

[7] Seo J. Y and Lee S.-I, "Predicting changes in spatiotemporal ground- water storage through the integration of multi-satellite data and deep learning models," *IEEE Access*, vol. 9, pp. 157 571-157 583, 2021.

[8] A. Wunsch, T. Liesch, and S. Broda, "Groundwater level forecasting with artificial neural networks: a comparison of long short-term memory (LSTM), convolutional neural networks (CNNs), and non-linear autoregressive networks with exogenous input (NARX)," *Hydrol Earth Syst Sci*, vol. 25, no. 3, pp. 1671–1687, Apr. 2021, doi: 10.5194/hess-25-1671-2021.

[9] S. Majumdar, R. Smith, J. J. Butler, and V. Lakshmi, "Groundwater Withdrawal Prediction Using Integrated Multitemporal Remote Sensing Data Sets and Machine Learning," *Water Resour Res*, vol. 56, no. 11, 2020, doi: 10.1029/2020WR028059.

[10] Grigsby Jake, Wang Zhe, Qi Yanjun, and Nguyen Nam, "Long-Range Transformers for Dynamic Spatiotemporal Forecasting," *eprint arXiv:2109.12218*, Sep. 2021.

[11] M. Sheykhmousa, M. Mahdianpari, H. Ghanbari, F. Mohammadimanesh, P. Ghamisi, and S. Homayouni, "Support Vector Machine Versus Random Forest for Remote Sensing Image Classification: A Meta-Analysis and Systematic Review," 2020. doi: 10.1109/JSTARS.2020.3026724.

[12] H. Yoon, S. C. Jun, Y. Hyun, G. O. Bae, and K. K. Lee, "A comparative study of artificial neural networks and support vector machines for predicting groundwater levels in a coastal aquifer," *J Hydrol (Amst)*, vol. 396, no. 1–2, 2011, doi: 10.1016/j.jhydrol.2010.11.002.

[13] T. Zhou, F. Wang, and Z. Yang, "Comparative analysis of ANN and SVM models combined with wavelet preprocess for groundwater depth prediction," *Water (Switzerland)*, vol. 9, no. 10, 2017, doi: 10.3390/w9100781.

[14] X. Huang, L. Gao, R. S. Crosbie, N. Zhang, G. Fu, and R. Doble, "Groundwater recharge prediction using linear regression, multi-layer perception network, and deep learning," *Water (Switzerland)*, vol. 11, no. 9, 2019, doi: 10.3390/w11091879.

[15] S. A. Naghibi, K. Ahmadi, and A. Daneshi, "Application of Support Vector Machine, Random Forest, and Genetic Algorithm Optimized Random Forest Models in Groundwater Potential Mapping," *Water Resources Management*, vol. 31, no. 9, 2017, doi: 10.1007/s11269-017-1660-3.

[16] D. Liu, A. K. Mishra, Z. Yu, H. Lü, and Y. Li, "Support vector machine and data assimilation framework for Groundwater Level Forecasting using GRACE satellite data," *J Hydrol (Amst)*, vol. 603, 2021, doi: 10.1016/j.jhydrol.2021.126929.

[17] Seo J. Y. and Lee S.-I., "Predicting changes in spatiotemporal ground- water storage through the integration of multi-satellite data and deep learning models," *IEEE Access*, vol. 9, pp. 157 571-157 583, 2021.

[18] A. Laouina, "PROSPECTIVE « MAROC 2030 » ," *Gestion durable des ressources naturelles de la biodiversite´ au maroc," Rapport pour le compte du HAUTCOMMISSARIAT AU PLAN ROYAUME DU MAROC*, 2006.

[19] T. L. machine learning on heterogeneous systems, "TensorFlow," 2015. [Online]. Available: https://www.tensorflow.org

[20] C. f, "keras-team/keras," 2015. [Online]. Available: https://github.com/fchollet/keras

[21] R. Vallat, "Pingouin: statistics in Python," *J Open Source Softw*, vol. 3, no. 31, 2018, doi: 10.21105/joss.01026.

[22] C. R. Harris *et al.*, "Array programming with NumPy," 2020. doi: 10.1038/s41586-020-2649-2.

[23] P. Virtanen *et al.*, "SciPy 1.0: fundamental algorithms for scientific computing in Python," *Nat Methods*, vol. 17, no. 3, 2020, doi: 10.1038/s41592-019-0686-2.

[24] F. Pedregosa *et al.*, "Scikit-learn: Machine learning in Python," *Journal of Machine Learning Research*, vol. 12, 2011.

[25] K. Jordahl *et al.*, "geopandas/geopandas: v0.8.1," *Zenodo*, 2020.

[26] pandas development team, "pandas-dev/pandas: Pandas 1.0.3," *Zenodo*, 2020.

[27] "Folium — Folium 0.11.0 documentation." [Online]. Available: https://python-visualization.github.io/folium/

[28] M. Waskom, "seaborn: statistical data visualization," *J Open Source Softw*, vol. 6, no. 60, 2021, doi: 10.21105/joss.03021.

[29] J. D. Hunter, "Matplotlib: A 2D Graphics Environment, Computing in Science & Engineering," *Comput Sci Eng*, vol. 9, no. 3, 2007.

[30] T. Chen and C. Guestrin, "XGBoost: A scalable tree boosting system," in *Proceedings of the ACM SIGKDD International Conference on Knowledge Discovery and Data Mining*, 2016. doi: 10.1145/2939672.2939785.

[31] G. I. S. O. S. G. F. QGIS Development Team QGIS, "Welcome to the QGIS project!," 2009. [Online]. Available: http://qgis.osgeo.org

[32] M. Amani *et al.*, "Google Earth Engine Cloud Computing Platform for Remote Sensing Big Data Applications: A Comprehensive Review," *IEEE J Sel Top Appl Earth Obs Remote Sens*, vol. 13, 2020, doi: 10.1109/JSTARS.2020.3021052.

[33] T. S. Steenhuis and W. H. Van Der Molen, "The Thornthwaite-Mather procedure as a simple engineering method to predict recharge," *J Hydrol (Amst)*, vol. 84, no. 3–4, pp. 221–229, May 1986, doi: 10.1016/0022-1694(86)90124-1.

[34] C. ,Warren Thornthwaite and J. R. Mather, "Instructions and Tables for Computing Potential Evapotranspiration and the Water Balance," *Laboratory of Climatology*, 1957.

[35] S. Majumdar, R. Smith, J. J. Butler, and V. Lakshmi, "Groundwater Withdrawal Prediction Using Integrated Multitemporal Remote Sensing Data Sets and Machine Learning," *Water Resour Res*, vol. 56, no. 11, Nov. 2020, doi: 10.1029/2020WR028059.

[36] M. Topuz and M. Deniz, "Application of GIS and AHP for land use suitability analysis: case of Demirci district (Turkey)," *Humanit Soc Sci Commun*, vol. 10, no. 1, 2023, doi: 10.1057/s41599-023-01609-x.

[37] N. Gorelick, M. Hancher, M. Dixon, S. Ilyushchenko, D. Thau, and R. Moore, "Google Earth Engine: Planetary-scale geospatial analysis for everyone," *Remote Sens Environ*, vol. 202, 2017, doi: 10.1016/j.rse.2017.06.031.

[38] C. Funk *et al.*, "The climate hazards infrared precipitation with stations - A new environmental record for monitoring extremes," *Sci Data*, vol. 2, 2015, doi: 10.1038/sdata.2015.66.

[39] T. Hengl and S. Gupta, "Soil water content (volumetric%) for 33kPa and 1500kPa suctions predicted at 6 standard depths (0, 10, 30, 60, 100 and 200 cm) at 250 m resolution (Version v01)," *Zenodo. Available at: https://zenodo. org/(Accessed 06 April 2022)*, 2019.

[40] A. G and recharge estimation using google earth engine Groundwater, "Google Earth Engine," 2022. [Online]. Available: https://developers.google.com/earth-engine/

[41] R. G. Allen, L. S. Pereira, D. Raes, M. Smith, and a B. W, "Crop evapotranspiration - Guidelines for computing crop water requirements - FAO Irrigation and drainage paper 56," *Irrigation and Drainage*, 1998, doi: 10.1016/j.eja.2010.12.001.

[42] He Tong and Chen Tianqi, "Xgboost: extreme gradient boosting," *R package version 0.4-2*, vol. 1, no. 4, 2015.

[43] J. H. Friedman, "Greedy function approximation: A gradient boosting machine.," *The Annals of Statistics*, vol. 29, no. 5, Oct. 2001, doi: 10.1214/aos/1013203451.

[44] T. Chen *et al.*, "Package 'xgboost,'" 2019.

[45] Y. Yang, R. J. Donohue, and T. R. McVicar, "Global estimation of effective plant rooting depth: Implications for hydrological modeling," *Water Resour Res*, vol. 52, no. 10, 2016, doi: 10.1002/2016WR019392.

[46] S. M. Basha and D. S. Rajput, "Chapter 9 - Survey on Evaluating the Performance of Machine Learning Algorithms: Past Contributions and Future Roadmap," Oct. 2019, *Academic Press*. [Online]. Available: https://www.sciencedirect.com/science/article/pii/B9780128167182000166

[47] C. S. J. Chu, "Time series segmentation: A sliding window approach," *Inf Sci (N Y)*, vol. 85, no. 1–3, 1995, doi: 10.1016/0020-0255(95)00021-G.

[48] T. C. Fu, "A review on time series data mining," 2011. doi: 10.1016/j.engappai.2010.09.007.